Single molecule force measurements of chitosan

Marta Kocun

A Thesis

in

The Department

of

Chemistry and Biochemistry

Presented in Partial Fulfillment of the Requirements
for the Degree of Master of Science (Chemistry) at
Concordia University
Montréal, Québec, Canada

November 2007

Your file Votre référence
ISBN: 978-0-494-40858-2
Our file Notre référence
ISBN: 978-0-494-40858-2

ABSTRACT

Single molecule force measurements of chitosan

Marta Kocun

Chitosan, a glucosamine polysaccharide derived form chitin, was studied by AFM-based single molecule force spectroscopy. The goal of this study was to investigate chitosan's adhesive properties to various surfaces (*i.e.* mica, glass, quartz, polytetrafluoroethylene and self-assembled monolayers) as well as obtaining its mechanical constants. The results obtained were in the form of force-extension curves and mathematical fits. Well-defined features, characteristic of single molecule adhesion and stretching, such as constant force plateaus and peaks, were observed in the force curves. The lengths of the constant force plateaus obtained are consistent with the lengths of chitosan strands observed in high resolution AFM images. The energy of desorption of single glucosamine residues from various surfaces was calculated. The values obtained were: 1.8×10^{-20} J/glucosamine residue on self-assembled monolayers of mercaptoundecanoic acid:dodecanethiol (1:1000), 2.0×10^{-20} J/glucosamine residue on quartz, 3.5×10^{-20} J/glucosamine residue on polytetrafluoroethylene and 3.9×10^{-20} J/glucosamine residue on self-assembled monolayers of dithiobis(succinimidyl undecanoate). The Kuhn length of chitosan (DDA 92%) was calculated, using the freely-jointed chain model, to be 2.1 ± 0.9 nm which corresponds to a stiffness of approximately 4 glucosamine residues. These single molecule level results could be applied towards the preparation of novel, chitosan-based biomaterials.

Acknowledgements

I would like to express my gratitude to my supervisors, Dr. Louis Cuccia and Dr. Michel Grandbois for their guidance and insight throughout my graduate studies. Particularly, I would like to thank Dr. Louis Cuccia for believing in my abilities and giving me a chance to work in his lab, for being enthusiastic about my research and, most importantly, for his friendship. I am thankful to Dr. Christine DeWolf and Dr. Cameron Skinner for agreeing to serve on my research committee and for their useful comments. I also acknowledge the assistance from my fellow graduate students, members of the Department of Chemistry & Biochemistry of Concordia University and the financial support provided by NSERC, Sigma Xi and CSACS.

My research experience at Concordia University would not have been the same without the people who surrounded me throughout my stay here. My thanks to Dr. Rolf Schmidt, with whom, daily *scientific discussions* shaped my outlook on research and life in general. James, thank you for sharing your *elder graduate student* wisdom, your optimistic view of the future and the ever entertaining lunches. Monica and Carolin, thank you for your moral support, your kindness, your craziness and your positive energy in the lab as well as in the office. Many thanks to the former and current members of the Cuccia and Grandbois labs for their help and friendship. I would like to thank my family and friends for their support and understanding. Special thanks to Jessica for her sense of humor and for the countless "*Jessica & Marta specials*" during my stay at Concordia.

Finally, this work would not have been possible without the constant encouragements, help, criticism, friendship and love of Thomas D. Lazzara. Thank you.

Table of contents

List of figures

List of tables

List of equations

List of abbreviations & symbols

AFM	atomic force microscopy
DDA	degree of deacetylation
DSU	dithiobis(succinimidyl undeacanoate)
FJC	freely-jointed chain
InvOLS	inverse optical lever sensitivity
k_B	Boltzmann constant
l_C	contour length
l_K	Kuhn length
l_P	persistence length
N	number of points in a population
NMR	nuclear magnetic resonance
PBS	phosphate buffered saline
PSD	power spectral density
PTFE	polytetrafluoroethylene
SAM	self-assembled monolayer
SD	standard deviation
SEM	scanning electron microscopy
SFA	surface force apparatus
SMFS	single molecule force spectroscopy
SPM	scanning probe microscopy
STM	scanning tunneling microscopy
T	temperature
THF	tetrahydrofuran
WLC	worm-like chain
$\bar{X}$	average value of a population of points
x	extension
Δ	phase shift
κ	spring constant
Φ	specific stiffness
Ψ	amplitude ratio

Chapter 1. Introduction

1.1. Goals of study

The general goal of this research is to characterize chitosan properties in relation to its interactions with different surfaces. Specifically, (*i*) the adsorption of single molecule strands of chitosan to biologically relevant surfaces will be studied and (*ii*) the mechanical properties/parameters of chitosan will be determined. Ultimately this new information will contribute to the general knowledge in the field of biophysical polysaccharide research. More specifically, this greater understanding of chitosan at the single molecule level will help the advancement of chitosan-based biomaterial research. AFM-based Single Molecule Force Spectroscopy (SMFS), a technique proven very successful in the study of numerous polysaccharides, was used in this study.

1.2. Polysaccharides

Carbohydrates are the most abundant class of natural products on earth. They are present among plants and animals in many forms and take part in countless vital roles. Carbohydrates are produced by microorganisms and plants, and are major components in shells of insects and crustaceans, in supporting tissues of plants and in cell walls.[1] A carbohydrate is defined as a polyhydroxy aldehyde or ketone, or any of their derivatives obtained by (*i*) reduction producing sugar alcohols, (*ii*) oxidation producing sugar acids, (*iii*) substitution of hydroxyl groups by hydrogen or amino groups to yield deoxysugars and amino sugars, respectively, (*iv*) derivatization of hydroxyl groups by sulfuric or

phosphoric acids to obtain sulfo- and phospho- sugars *or* reaction of the hydroxyl groups with alcohols to obtain monosaccharides, oligosaccharides and polysaccharides.[2]

Monosaccharides are chemical units with a general formula $C_n(H_2O)_n$. In Figure 1, a glucose monosaccharide is shown with conventional numbering of the carbon atoms.

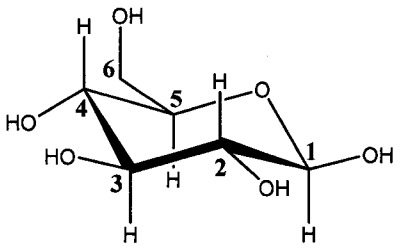

Figure 1. Glucose monomer with numbered carbons

The term oligosaccharide is used to define a compound where two or more monosaccharides are joined by glycosidic linkages. Depending on the number of monosaccharides joined together, the oligomers obtained can be disaccharides (*e.g.* sucrose) (Figure 2) trisaccharides (*e.g.* raffinose), tetrasacchardies (*e.g.* stachyose), *etc.*

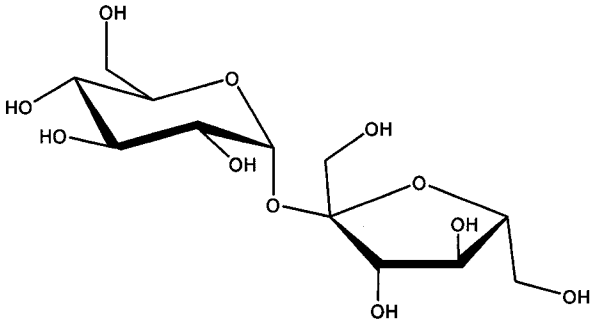

Figure 2. Sucrose, a disaccharide composed of glucose and fructose monomers

The configuration of the glycosidic bond can be α (axial) or β (equatorial) and is present between any of the alcohol groups at either carbon 2, 3, 4 or 6. Examples of the glycosidic linkages present in various polysaccharides are shown in Figure 3: mannose

(α(1-4) linked D-glucopyranose units), chitosan (β(1-4) linked D-glucose units), dextran (α(1-6) linked D-glucopyranose units) and gentiobiose (β(1-6) linked D-glucose units).[2,3]

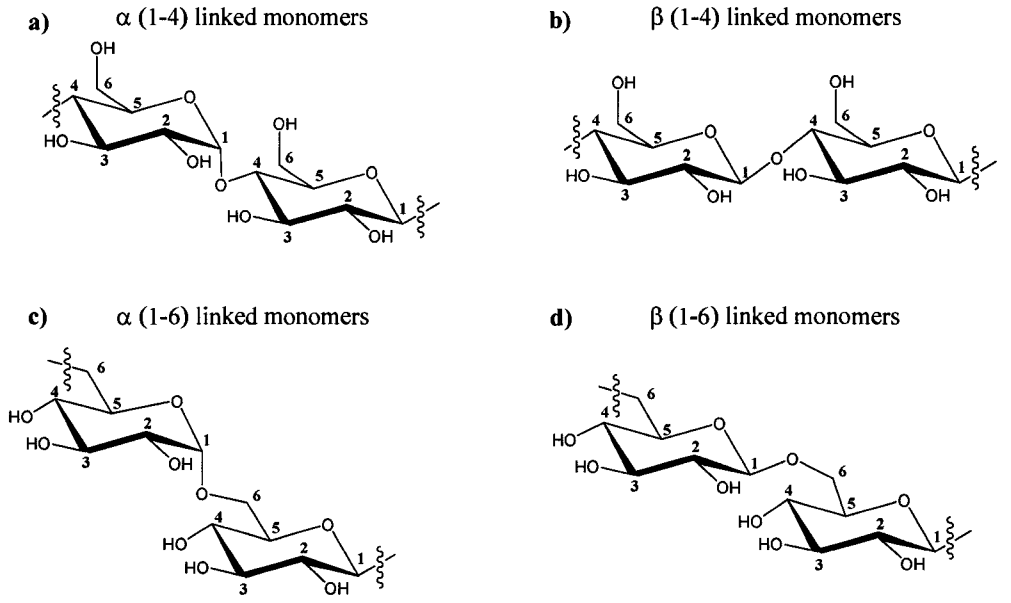

Figure 3. Glycosidic linkages in various polysaccharides

Polysaccharides are simply long oligosaccharides. Because their length is polydisperse, an average molecular weight rather than a single molecular weight is typically used to describe polysaccharides. Starch, glycogen, cellulose and chitin are the most abundant polysaccharides in nature. Starch is synthesized by plants as an energy storage molecule. The polymer consists of a polysaccharide built from both α-amylose, which is a linear polymer of α(1-4) linked glucose monomers, and amylopectin which is a polymer of α(1-4) linked glucose monomers branched every 24-30 monomers by α(1-6) bonds. Glycogen plays an energy storage role in animals and this polysaccharide structure is similar to amylopectin with the exception of branching in the latter which takes place every 8-12 glucose monomers. Cellulose is the basic building block that

provides structural support to plants and is a β-isomer of amylose consisting of β(1-4) linked glucose monomers. Chitin is a similar homopolymer of β(1-4) linked *N*-acetyl-D-glucosamine residues and is nature's second most abundant polysaccharide next to cellulose.[1,4] Chitin is the structural component of the exoskeletons of invertebrates such as crustaceans, insects and spiders and is also found in fungi and algae. Aside from its role in biological systems, chitin applications are limited because of its low solubility in aqueous solutions. The focus of this thesis is on chitosan, a derivative of chitin, which has been widely exploited for its properties in biomedical, nutritional, cosmetic and other industries.

1.3. Chitosan as a biomaterial

Chitosan is a linear cationic polysaccharide composed of β(1-4) linked glucosamine and *N*-acetyl glucosamine monomers and is obtained by the *N*-deacetylation of chitin under basic conditions (Figure 4).[5]

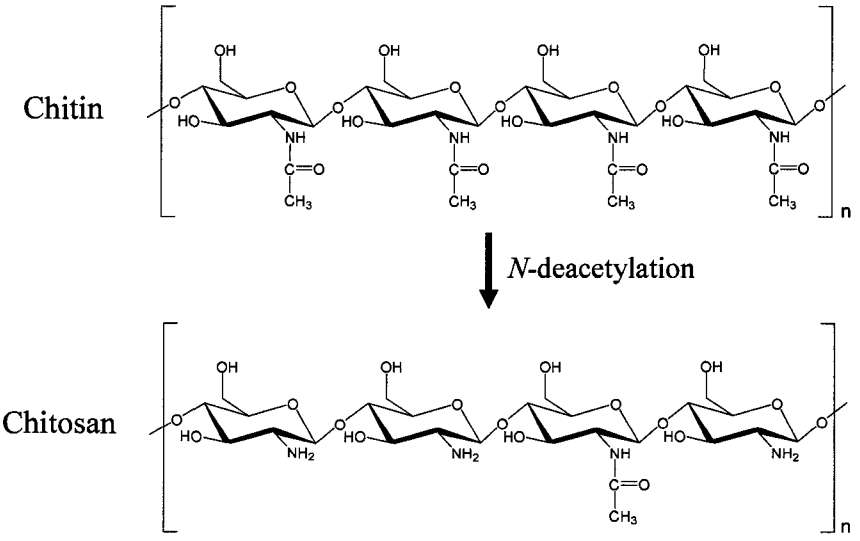

Figure 4. Chitosan is obtained by *N*-deacetylation of chitin

Chitosan is soluble in slightly acidic solution and its properties, which include biocompatibility, nontoxicity and biodegradability, make it an ideal candidate for use in biomedical applications. Chitosan and chitosan derivatives have been used as cartilage replacement materials, scaffolds for cell growth as well as bioactive coatings for dental and craniofacial implants.[6-8] Chitosan and its derivatives are also being tested in drug delivery systems and as humidity retention additives in some cosmetics.[9,10] Recently, Kujawa *et al.* prepared viscoelastic biocompatible hyaluronan and phosphorylcholine-modified chitosan films which have the potential to be used as biocompatible surface coatings.[11]

The properties of chitosan are highly dependent on its degree of deacetylation (DDA) (Equation 1).

$$\%\,\mathrm{DDA} = \text{degree of deacetylation} = \left(\frac{\text{amino groups}}{\text{total sugar units}}\right)\times 100$$

Equation 1. Degree of deacetylation (DDA) of chitosan

For example, in a polysaccharide composed of 100 monomers, chitosan with a DAA of 98% would have 98 monomers with amino groups at carbon 2 and two monomers with acetyl groups at carbon 2. Chitosan has been characterized by ^{1}H-NMR, gel permeation chromatography and infrared spectroscopy.[12-14] The intrinsic pKa of chitosan varies between 6.5 and 7.5 depending on the DDA (*i.e.* the chemical environment changes with the degree of amine substitution).[15,16] Besides the DDA, chitosan's behavior is influenced by its molecular weight, by temperature, where the viscosity increases as the temperature increases. Buschmann and coworkers exploit this property in cartilage repair applications where chitosan mixtures, liquid at room temperature, is injected into the joints and as the

temperature increased to 37°C, the chitosan mixture solidifies into a cartilage like texture.[17,18] Many studies have been performed to elucidate chitosan's properties in bulk (*i.e.* viscosity, chain rigidity, fat binding capacity, *etc.*)[10,19,20] and as part of more complex systems but very few investigate chitosan at the single molecule level.[6,16,21]

The main goal of this thesis is to study the behavior of chitosan at the single molecule level, to obtain microscopic parameters inaccessible by current studies based on macroscopic samples.[19,22] Force spectroscopy, based on Atomic Force Microscopy (AFM) was used in the present research to study the properties of chitosan polymer molecules. The interaction of chitosan with various surfaces was studied. A better understanding of this biopolymer is expected to allow for the design of novel chitosan-based biomaterials.

1.4. Single molecule force measurements

1.4.1. Current single molecule force techniques

There are many single molecule manipulation methods available, based on: (*i*) the principle of a probe which generates or detects forces and displacements and, (*ii*) a setup which allows the spatial location of the molecules being studied. The methods can be separated into mechanical transducers and external field manipulators. Mechanical transducers can be cantilevers or microneedles and external field manipulators consist of magnetic fields and photon fields.[23] Depending on the systems studied, each technique has its advantages and disadvantages. Bustamante *et al.* have compared the range of forces that can be studied with each of the methods. Some applications and practical advantages/disadvantages of these techniques are given in Table 1.[23]

Table 1. Single molecule force measurement techniques[23,24]

Technique	Force range	Dynamic range	Application	Advantages & Disadvantages
Cantilevers	> 1	≥ 10 μs	- Proteins - Polysaccharides - Bond strength	+ High spatial resolution - Fragile and costly
Microneedles	> 0.1	≥ 100 ms	- DNA - Proteins	+ Delicate enough for biological systems - Not commercially available
Magnetic beads	0.01 – 100	≥ 1 s	- Stretching and twisting DNA	+ Ability to induce torque - Indirect measurement of magnetic forces
Optical tweezers	0.1-150	≥ 10 ms	- Protein unfolding - Protein motors	+ Direct high resolution force and position measurements - Laser damage to biological systems

AFM-based single molecule force spectroscopy was chosen for this study of chitosan properties due to its high resolution imaging, its pN force detection and its versatility in terms of probe and sample preparation. It is a mechanical transducer method in which a cantilever is used to generate forces on a molecule of interest and a photodetector is used to amplify the movement of the cantilever into a signal which is then converted into a force. Section 1.4.2 provides a detailed discussion of the AFM-based force spectroscopy technique essential to this thesis.

1.4.1.1. Optical tweezers and magnetic beads

Optical tweezers, also referred to as optical traps, were first experimentally applied by Ashkin *et al.* in 1986 where the trapping of dielectric particles ranging in size from 25 nm to 10 μm was reported.[25] The operating principle of the optical trap lies in the radiation pressure which is a force created by a change in momentum of light. This change in momentum is due to the refraction and reflection of light from the particle

being studied. The radiation pressure is provided by the laser light.[26] Figure 5 illustrates the forces acting on the particle; the particle is 'pulled' by the refraction of light and 'pushed' by the reflection of light from the surface of the particle. It is the sum of the two opposing forces that is responsible for the optical trapping of particles.

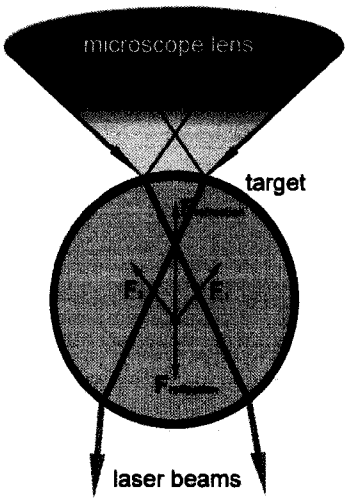

Figure 5. Schematic representation of an optical trap (image adapted from ref. 26)

The optical tweezers setup consists of two parts; one is stationary and holds the particle in place, while the other is mobile and allows for the application of force. The stationary region can be a surface to which a molecule is covalently attached (Figure 6a) or it could also be a pipette which holds a bead to which a molecule is linked (Figure 6b). The optical trap serves as the mobile region.

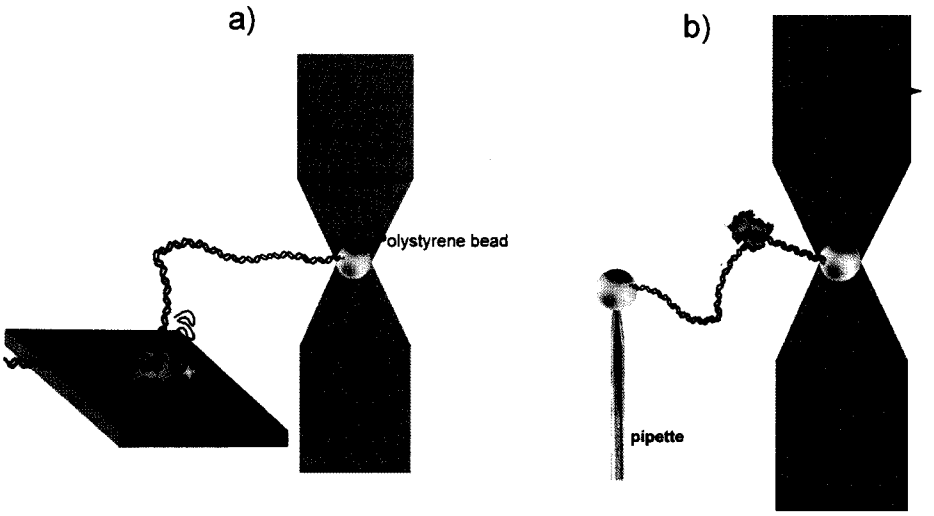

Figure 6. Schematic representation of optical tweezers where a) a surface is used as a stationary phase and b) a pipette is used as a stationary phase

A trap can also be created from two focused laser beams as shown in Figure 7. This optical trap can generate higher forces but the setup is more complex.

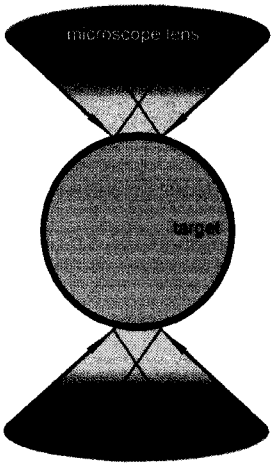

Figure 7. Schematic representation of a dual beam optical trap (image adapted from ref. 26)

Regardless of the setup being used, the force is determined in the same way. When a bead is held some distance away from the focus of the laser beam it is pulled towards it. This

pulling force is proportional to the distance between the center of the bead and the focal point. According to Bustamante *et al.*, the force can be determined when the trap stiffness (k) and the bead's position (x) are known.[23]

$$F = -k\,x$$

Equation 2. Pulling force in optical tweezers

Image analysis is used to determine the bead's position with up to 10 nm accuracy. The trap's stiffness (*i.e.* the force needed to displace a bead in the trap) is dependant on the optical design of the system and the size of the bead. A stiffness of 50 pN/μm yields 0.5 pN resolution in force measurements. Carlos Bustamante pioneered the use of optical tweezers to study the mechanical properties of biomolecules. For example, forces necessary to unfold and fold the protein titin, as well as the hysteresis of the events were measured with the use of optical tweezers.[27] Unfolding forces ranged between 20 and 30 pN and the refolding forces were as low as 2.5 pN. In 2003, the strength and locations of kinetic barriers opposing the unfolding of single molecules of a derivative of *T. thermophilia* ribozyme and RNA were studied.[28] Discrete events which lasted for several seconds were observed and correspond to the intra- and interdomain interactions (10-30 pN).

Similarly to optical tweezers, magnetic tweezers are comprised of stationary and mobile regions. The system under study is anchored to a surface at one end and is attached to a magnetic bead at the other end. In the optical tweezers setup, a photon field is used to apply a force to the system. Here however, the photon field is replaced by a magnetic field generated by electromagnets. Smith *et al.* studied DNA's elasticity using

magnetic beads and forces ranging from 0.01 pN to 10 pN were applied to the DNA where the tension and elongation of the strands in response to the applied force was measured.[29]

1.4.1.2. Surface force apparatus

The surface force apparatus measures the force between two cylindrically curved surfaces that are moving into close contact. The surfaces are held 90° to each other creating a 'cross cylinders geometry' which is mathematically equivalent to the interaction of a sphere with a flat surface. The first Surface Force Apparatus (SFA) measurements were performed by Tabor and Winterton in 1969.[30] Their experiment measured the van der Waals force between two mica surfaces in air. It was later Israelachvili and Tabor in 1972 and Israelachvili and Adams in 1978 that perfected the instrument so that the experiments could be performed in liquid.[31,32] The experimental setup is comprised of: (*i*) two surfaces, (*ii*) a mechanism which allows for their separation and approach, (*iii*) a device to measure the separation and (*iv*) a device to quantify the forces generated. The experimental setup of a typical SFA is shown in Figure 8.

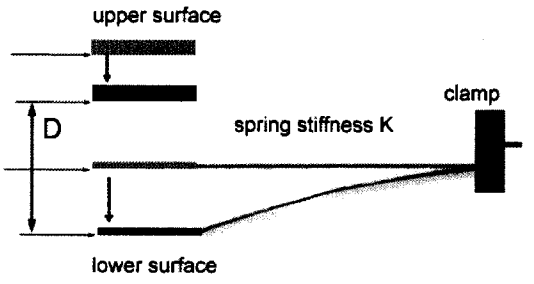

Figure 8. Schematic representation of a surface force apparatus (SFA). The initial positions of the surfaces is shown in grey. The upper surface is approached to the lower surface and the spring deflects downward. The final position of the surfaces is shown in black. D is the final distance separating the two surfaces (image adapted from ref. 31)

The separation of the surfaces is achieved using various motors, piezoelectric crystals and springs. The distance between the two surfaces is measured by monitoring the change in the intensity and shape of the interference fringes with a spectrometer. The force between the two surfaces is measured by reversing the voltage of the piezo which then contracts or expands and results in a new separation distance between the surfaces. The new position is measured optically and the difference between the initial and final separation is multiplied by the stiffness of the spring to obtain the force. Schob and Cichos introduced a SFA setup modified with a fluoresecence microscope to track single dye molecules.[33] This new application of SFA provides a powerful method for studying molecular motion in confined liquid films.

1.4.1.3. Microneedles

Force measurements by microneedles were first introduced by Kamimura and Takahashi in 1981.[34] In their study of microtubule sliding forces, sea-urchin sperm was attached to two polylysine coated glass microneedles. One of the microneedles was much stiffer and served as a static support, and the other, more flexible microneedle, was used to measure the sliding forces. When the microtubles slid apart, the flexible microneedle bent and the force corresponding to that deflection was calculated (Figure 9). The compliance of the microneedles used in the experiments was determined by calibration against a microneedle of known elastic coefficient (*ca.* 100 pN μm^{-1}).

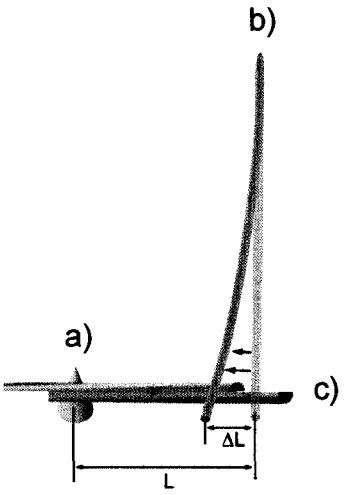

Figure 9. Schematic representation of a microneedle experiment. a) stiffer microneedle serving as static support, b) flexible microneedle used to measure the force, c) the two microtubes sliding apart. L is the initial diastance between the two microneedles, ΔL is the extent of microneedle deflection (image adapted from ref. 35)

Kishino *et al.* used a modified microneedle set up to measure the tensile strength of a single actin filament. The stiff glass microneedle was used to pull on the filament and the deflection of the flexible microneedle was used to measure the tensile strength. The extent of microneedle bending was monitored by fluorescence force microscopy.[35] The elasticity of the microneedles used in this tensile strength study of actin filaments was much smaller than the microtubule study, ranging between 1.5 and 10 pN μm^{-1}.

1.4.2. AFM Single molecule force spectroscopy

The invention of the scanning tunneling microscope by Binnig and Röher in 1982 earned them the 1986 Nobel Prize in Physics and initiated the development of the scanning probe microscopies. Scanning Probe Microscopes (SPM), such as Scanning Tunneling Microscopies (STM) and Atomic Force Microscopes (AFM), are instruments where a physical probe is scanned, in a raster fashion, over a surface to characterize it.

The advantage of SPM techniques compared to the conventional optical imaging methods is the ability to probe a surface feature in three dimensions *x, y* and *z*. In STM, electrons 'tunnel' between a tip and a conductive sample producing a current which is used to create an atomic-scale image of the surface.[36,37] AFM, developed by Binnig, Quate and Gerber in 1986[38], uses a soft spring cantilever to probe surface features and topology at the molecular level. If, during an AFM experiment, *x, y* and *z* dimensions are explored simultaneously, a topographic picture of the surface at the nanometer scale is obtained, but when the experiments are conducted only in the *z* direction, force curves are obtained.

AFM images can be obtained in different modes. Contact mode and intermittent contact mode (Digital Instruments' Tapping Mode®), are the two main methods of surface imaging. During contact mode imaging (Figure 10 a), a small constant force is exerted on the cantilever where a tip is located. The tip is raster scanned over the surface during which a feedback loop assures a constant tip-surface separation. Changes in the deflection of the cantilever are recorded and used to create a three-dimensional image of the surface. In intermittent contact mode the cantilever oscillates close to its resonance frequency (Figure 10 b). The amplitude, phase and the resonance frequency of the cantilever are modified by the interaction forces between the tip and surface. These changes in oscillation provide a feedback signal which is used to maintain a constant height and produce a three-dimensional image of the surface similar to the contact mode imaging but with minimal shear forces applied to the sample.

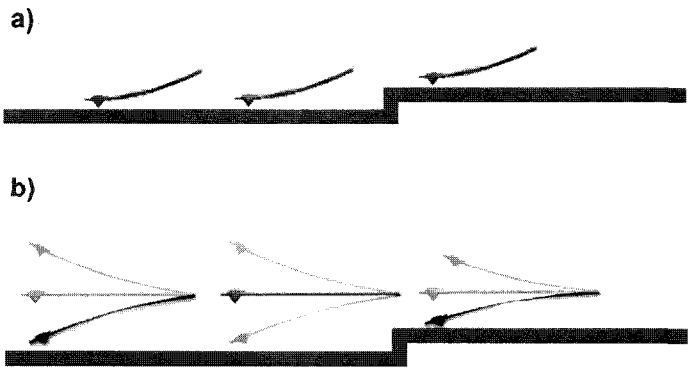

Figure 10. AFM imaging modes: a) contact mode and, b) intermittent contact mode

AFM force curves are obtained by probing the surface only in the *z* direction. Whether performing surface imaging or obtaining force curves, both experiments make use of the same SPM tip: a very small pyramidal tip with a radius of curvature at the apex as small as 20 nm, (Figure 11) located on a soft spring cantilever which interacts with the surface.

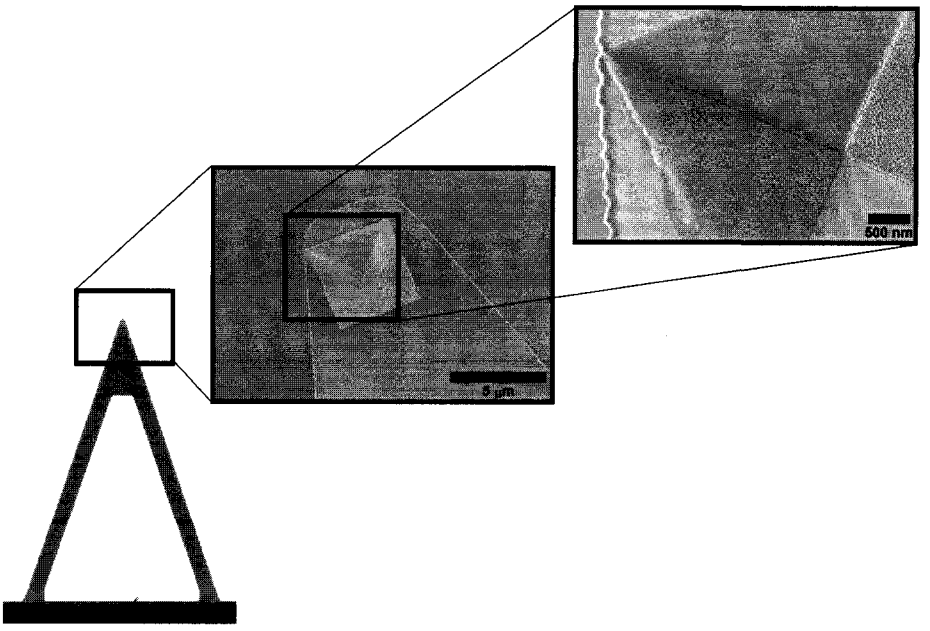

Figure 11. Silicon nitride AFM probe (from left: optical microscope image, two SEM images)

When the tip interacts with the surface the cantilever deflects because of its flexibility. This deflection is monitored *via* the displacement of a laser beam reflecting from the back of the reflective cantilever onto a position sensitive photodiode (Figure 12).

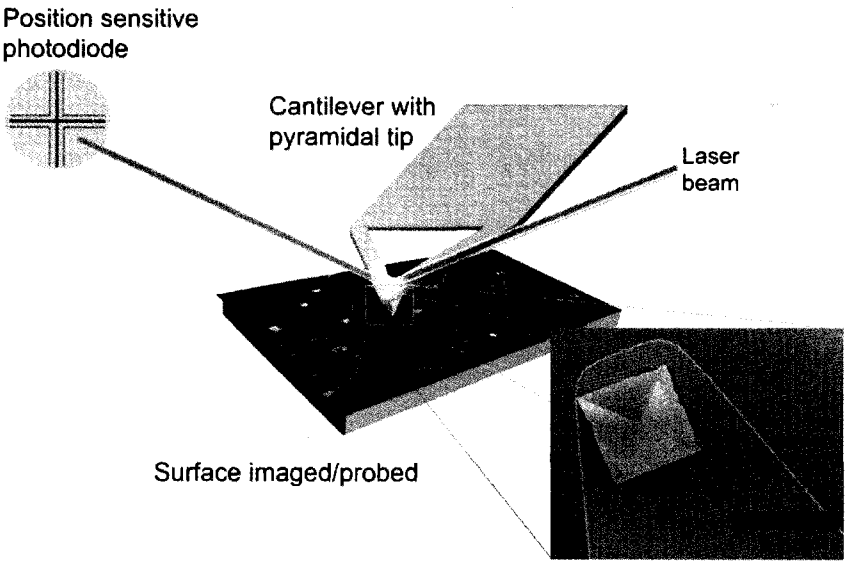

Figure 12. AFM force-detection scheme

The interaction force is obtained by multiplying the deflection of the cantilever by its spring constant. Spring constant calibration can be conducted by static methods which include: (*i*) the *calibrated cantilever method* and (*ii*) the *static added-mass method* or by dynamic methods such as: (*iii*) the *dynamic added mass method,* (*iv*) *the thermal noise method* and (*v*) the *unloaded frequency method.*[39,40,41] The thermal noise method is used to calibrate the cantilevers in all of the experiments presented in this thesis.

A typical force curve is shown in Figure 13. The experiment starts with the tip far away from the surface (Figure 13, part 1). It is then slowly approached (following the red trace) until it makes contact with the surface (Figure 13, part 2). A force can then be

applied to the sample by pushing the tip into the surface (Figure 13, part 3). The retraction curve is shown in blue. The force needed to overcome the interaction between the tip and the surface is observed in the form of a force peak (Figure 13, part 4). When there are no more interaction forces, the retraction curve returns back to baseline (Figure 13, part 5).

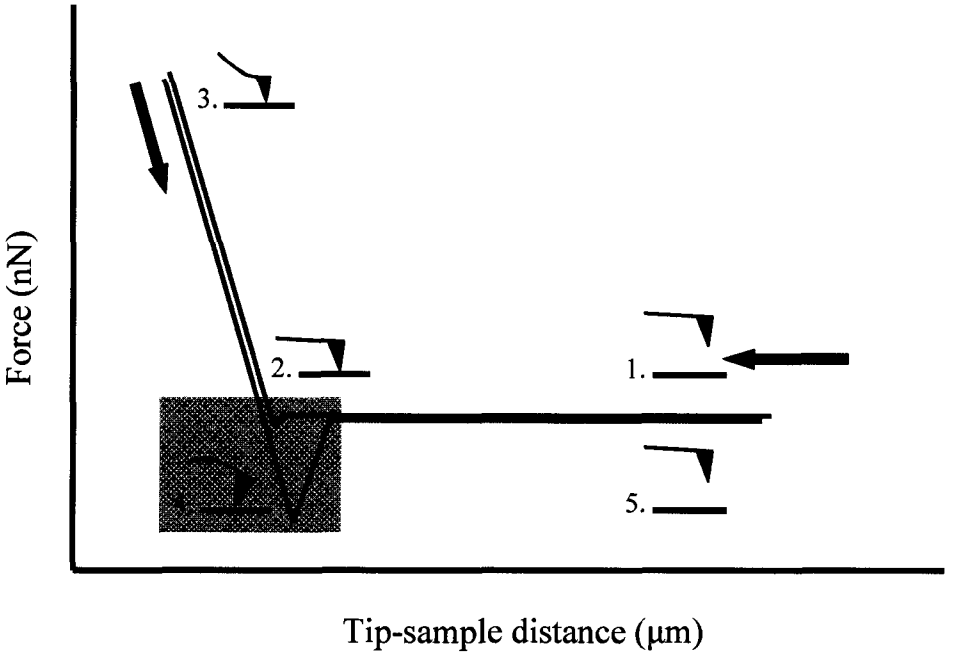

Figure 13. Features of a typical force curve. In red, the approach part of the force curve is shown with schematic representations of 1) AFM tip far away from the surface, 2) AFM tip making contact with the surface, 3) AFM tip pushing into the surface. In blue, the retraction part of the force curve is shown with schematic representations of 4) AFM tip adhesion to the surface and 5) AFM fully retracted from the surface to the initial position

The approach trace is of no interest to this research. The focus of this thesis is on the analysis of the retraction force curves. Each retraction curve is composed of regions containing information about the progress of the force curve and the molecular properties being studied. A schematic representation of these particular regions as well as the possible tip-surface interactions are depicted in Figure 14. The forces responsible for

these interactions include ionic interactions, ion-dipole interactions, dipole-dipole interactions, hydrogen-bonding forces, solvent ordering double layer formation and van der Waals forces.[42,43,44] Close range interactions experienced by the tip (Figure 14, region a) are difficult to analyze because of the proximity of the tip to the surface. Stretching of the polymer begins as soon as the tip is retracted (Figure 14, region b). This part of the curve contains information that pertains to the elasticity of the polymer being studied. Mathematical models (described below), are used to extract valuable information from this part of the force curve. As the tip is further retracted from the surface, the polymer stretches until it is fully extended (Figure 14, region c), at which point conformational transitions can be observed for some molecules. [3,45,46-48,]

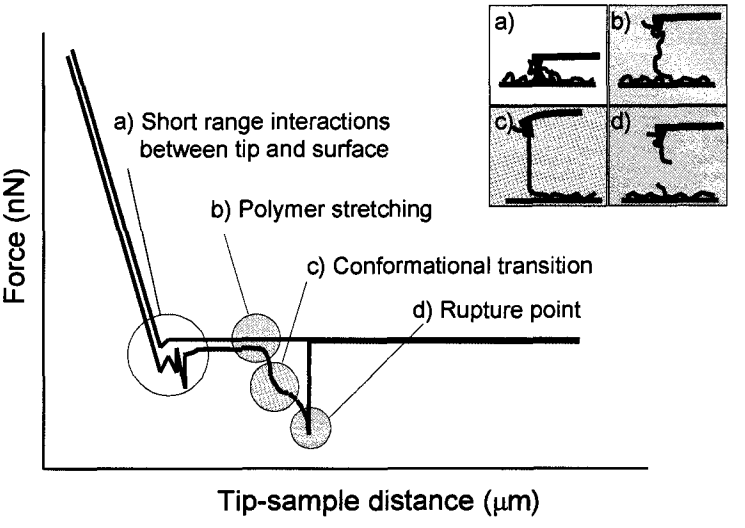

Figure 14. Regions of interest in a typical force curve for polymer physisorbed on a surface. The inset shows a schematic representation of the AFM tip position in relation to the surface.

Finally, when the tip retraction continues, the rupture point is reached. This region (Figure 14, region d) corresponds to the desorption of the polymer from the tip (or surface) or covalent bond rupture in the polymer. At this point, there is no longer

bridging between the tip and the surface which is shown as the trace returns to the baseline.

The retraction curve contains the 'mechanical fingerprint' of the studied molecule. Single point desorption force peaks and constant force desorption plateaus are the main interest when analyzing retraction curves. Force peaks represent the point-desorption or point-rupture of the polymer being studied. Constant force plateaus, such as the one shown schematically in Figure 15, are another feature encountered during force spectroscopy experiments.

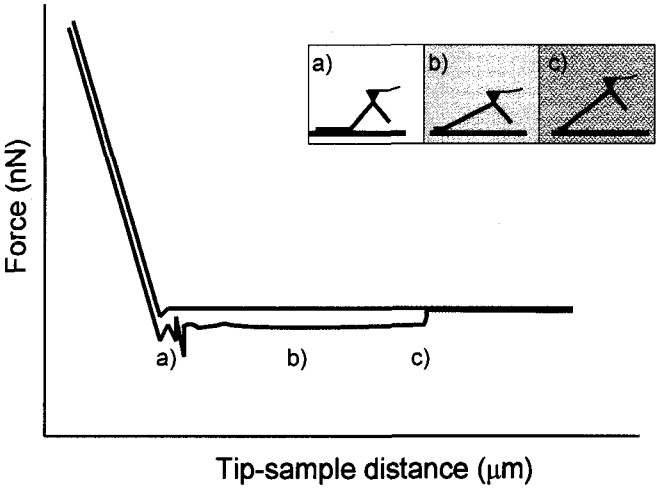

Figure 15. A force curve with a constant force plateau feature. The inset shows a schematic representation of the AFM tip position in relation to the surface.

Constant force plateaus represent the constant force needed to desorb a molecule which is uniformly spread on the surface. The plateau height indicates the force needed to desorb the molecule and the length represents the fraction of the molecule that is being desorbed (*i.e.* peeled) from the surface. Plateaus with multiple steps are often observed and they represent simultaneous desorption of more than one evenly spread strand from the surface.[49-54] Plateaus have been observed in several single molecule studies. Long *et al.* observed plateaus while studying the desorption of partially hydrolyzed polyacrylamide

from mica, silicon and bitumen surfaces.[55,56] Plateau lengths were in the hundreds of nanometers and the forces on mica, silica and bitumen were respectively 200, 40 and 80 pN in deionized water and 100, 50 and 40 pN when the experiments were performed in plant processed water. The authors assigned the plateau feature to the desorption of the polyacrylamide polymer which has a 'trainlike' conformation on the surface.

As mentioned previously, experimentally obtained force curves contain a variety of information about the polymer being studied: (*i*) desorption force from the surface, (*ii*) lengths of molecular strands as well as (*iii*) unique fingerprints in the retraction trace of force curves. In addition to the information just mentioned, mechanical properties of polymers can be obtained by using mathematical fitting models. The Freely Jointed Chain (FJC) (Equation 3) and the Worm-Like Chain (WLC) (Equation 4) are two main models used for single polymer curve fitting.[57,58] Mechanical properties of polymers are often defined through polymer constants such as contour length l_C, persistence length l_P, and Kuhn length l_K. Contour length corresponds to the linear length of a polymer without stretching its molecular backbone; persistence length is the flexibility of a polymer, it also corresponds to the shortest linear part of a worm-like chain molecule. Kuhn length is the measure of the stiffness of polymer segments in the FJC model of a polymer. When the Kuhn length is similar to the monomer length, the polymer is very flexible since the only limitation of its movement is the monomer itself. When the value of the Kuhn length is higher, the polymer is stiffer.

The FJC model applies to a polymer built of n rigid elements of Kuhn length (l_K) connected through flexible joints (Figure 16).

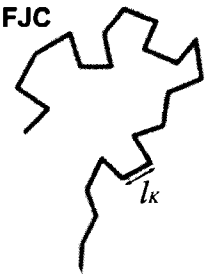

Figure 16. Representation of a polymer chain according to the FJC model.

Kuhn length defines the stiffness of a polymer segment, T is the temperature and k_B is the Boltzmann constant. Contour length (l_C) is the linear length of the extended molecule without stretching its molecular backbone. In force spectroscopy experiments, the tip randomly picks up only a part of a molecule therefore the contour length corresponds to a section of a whole molecule. The FJC has been used to model oligonucleotides and synthetic polymers (*e.g.* polydimethylsiloxanes, polymethacrylate).[58]

$$x(F) = l_C \left[\coth\left(\frac{Fl_K}{k_B T}\right) - \frac{k_B T}{Fl_K} \right]$$

Equation 3. Equation of FJC model

The WLC model applies to a polymer which can be described as a continuous string of constant elasticity (Figure 4). The persistence length (l_P) is the flexibility of the molecule, x is the extension and l_C, the contour length. Persistence length is related to Kuhn length by $l_P = l_K/2$.[58]

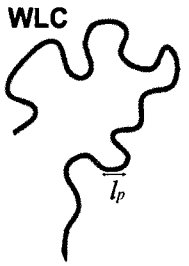

Figure 17. Representation of a polymer chain according to the WLC model

The WLC model has been successfully used to model the behavior of DNA, muscle, adhesion proteins and polymethacrylic acid.

$$F(x) = \frac{k_B T}{l_P}\left[\frac{1}{4}\left(1-\frac{x}{l_C}\right)^{-2} + \frac{x}{l_C} - \frac{1}{4}\right]$$

Equation 4. Equation of WLC model

FJC and WLC models consider only the entropic deformation of a polymer. The entropic deformation is the amount of motion that the chain can explore driven by temperature (k_BT) and this applies only to the initial increase of the force curve. In order to include the enthalpic deformation (elastic deformation), κ (spring constant of individual segments) is included in the FJC model and Φ (specific stiffness of a polymer) is incorporated in the WLC model.

$$x(F) = l_C\left[\coth\left(\frac{Fl_K}{k_B T}\right) - \frac{k_B T}{Fl_K}\right]\left(1+\frac{F}{\kappa l_C}\right) \qquad F(x) = \frac{k_B T}{l_P}\left[\frac{1}{4}\left(1-\frac{x}{l_C}+\frac{F}{\Phi}\right)^{-2} + \frac{x}{l_C} - \frac{F}{\Phi} - \frac{1}{4}\right]$$

Equation 5. Extended FJC model and extended WLC model respectively

1.4.3. Biomolecules studied with single molecule force spectroscopy

Within the past two decades, Single Molecule Force Spectroscopy (SMFS) has become a powerful tool for the investigation of biomolecules.[58] DNA, proteins and polysaccharides have been probed, stretched, pushed and pulled with the purpose of gaining information about their chemical and physical properties.

Lee *et al.* first studied double stranded DNA dissociation forces in 1994.[59] The forces were measured for 20, 16 and 12 base pair long DNA duplexes and the dissociation forces were 1.52, 1.11 and 0.83 nN, respectively. Later experiments with improved instrumentation performed by Rief *et al.* resolved G-C base pair dissociation and A-T base pair dissociation with forces of 20 pN and 9 pN, respectively.[60-62] Recently, an explanation for the force variation observed in various studies, has been proposed by Vander Wal *et al.*[63] According to their experimental work, DNA unbinding depends on the contact force of the tip probing the DNA sample, as well as on the ionic strength of the solution.

The first mechanical unfolding experiments of the multi-domain titin protein, a giant sacromeric protein of striated muscle, were carried out in 1997 by Rief *et al.*[64] Force curves of single molecules of titin exhibited a characteristic sawtooth pattern. The force peaks, which varied from 150 to 300 pN, were separated by 25-28 nm. The authors attributed this sawtooth pattern to the successive unfolding of titin domains. These experiments gave insight not only into the mechanical nature of this biomolecule but also into the structural information relative to protein folding. Protein characterization has been extended by combining AFM imaging with SMFS to study membrane proteins. Muller *et al.* stretched, unfolded and extracted the hexagonally packed intermediate (HPI)

layer of *Deinococcus radiodurans*, a bacterial surface protein. HPI layer pores, comprised of six interlinked promoters, were pulled out of the membrane with the AFM tip and the membrane was subsequently imaged to observe a vacant spot created by the extraction.[65] Oesterhelt *et al.* proceeded in the same manner to study the extraction of the bacteriorhodopsin membrane protein.[66] The forces anchoring the protein, composed of seven α-helices, were in the range of hundreds of pN. In contrast to the titin protein, where the forces increased as the stronger domains unfolded last, here the α-helices are destabilized by the removal of the helices and the forces decreased as the experiment progressed.

SMFS can also be used to probe the mechanical properties of polysaccharides. In 1999 Marszalek *et al.* found that the number of conformational transitions observed in force curves correspond to the number of axial glycosidic linkages found in the sugar polymer.[46-48] Pectin, amylose and cellulose were the pyranose-based, (1-4) glycosidic linked polymers used in their study. Two transitions were visible in pectin's force curves: at 300 pN and at 800 pN, due to a sequential chair inversion reaction. Zhang and Marszalek later showed that force spectroscopy can provide both the number and the specific location of axial linkages in pyranose rings.[67] They compared β-galactan, a β(1-4) linked D-galactose polysaccharide, with amylose, a α(1-4) linked D-glucose polysaccharide. Both of these polysaccharides have one axial and one equatorial bond but the order in which they are stretched is opposite for β-galactan (C_1 equatorial - C_4 axial) and amylose (C_1 axial - C_4 equatorial) (Figure 18).

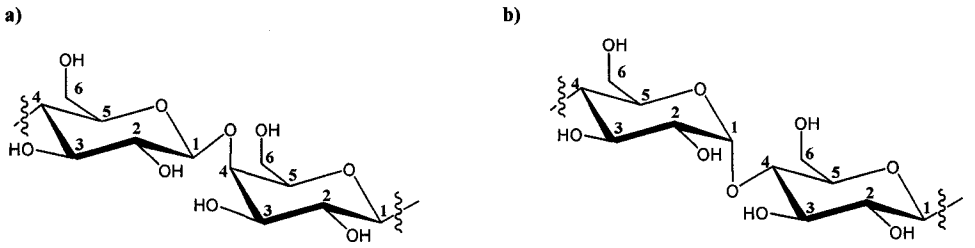

Figure 18. Glycosidic linkages in a) β-galactan and b) amylose

Plateaus of the same length but with different heights were observed for both sugars. In the case of the β-galactan the plateau height was 640 pN and for amylose the plateau height was 280 pN. The authors proposed that force spectroscopy could be used for mechanical identification of these sugar isomers.

Other polysaccharides were also studied by single-molecule force spectroscopy. Xanthan, an extracellular bacterial polysaccharide used in the food industry and for oil recovery, has a linear cellulosic backbone which adapts a helical secondary structure. Stabilized by non-covalent bonds, the native helical structure of xanthan can be denatured into a single stranded disordered state. Force spectroscopy studies show that when native xanthan is stretched, a 400 pN constant force plateau is visible.[61] However, when denatured xanthan was subjected to force spectroscopy, no features were observed in the force curves (*i.e.* there were no plateaus). The authors suggest that the plateau observed during stretching of native xanthan corresponds to changes in the helical conformation of the secondary structure of xanthan.[68] Force curves of dextran show a single transition at 850 pN which allows for an increase in its length by *ca.* 18%. This transition, also observed in pullulan (Figure 19), which is composed of α(1-4) and α(1-6) linked D-glucopyranose units,[3] is attributed to the force induced flipping of the pyranose ring from a chair to boat conformation confirmed by molecular mechanics calculations[47].

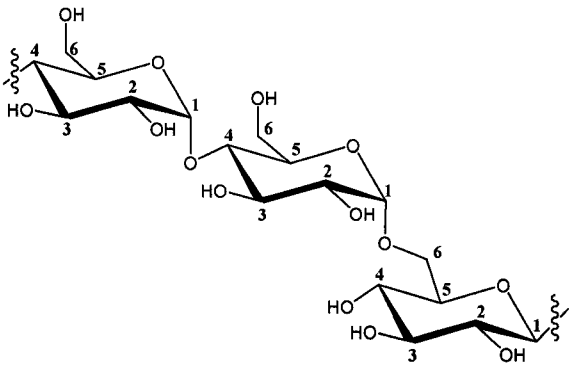

Figure 19. Structure of Pullulan

There are no single molecule force spectroscopy studies of chitosan reported in the literature which is a key motivation for this current investigation.

1.5. Surfaces as biointerfaces

An interface is the meeting point of two phases which can either be liquid, solid or vapor. A biointerface is where interfaces come into contact in a biological context. Biointerfaces are of key importance in research areas relating to implants, biosensors, drug delivery and coatings of various types.[69,70] Because the initial contact of a device with the host is the determining step of acceptance or rejection of the device by the host, properties of biointerfaces are crucial to any host-device interaction. Surface chemistry, surface energy, surface charge and surface structure all affect the biomaterial performance.[71] Performance of the implant is critical for patient well-being. For example, implants that are used for knee or hip replacements have different standards than implants used for crano-facial reconstruction. The first type, should have great resistance to sheer, pressure and friction, while the later should be soft, spongy and elastic.[8] Similarly, in

some cases the interaction at the biointerface should be weak and in other cases it should be strong. For example, a joint interface (*e.g.* knee or hip replacement) requires low friction interactions whereas dental implants require strong adhesiveness.

Single molecule force spectroscopy can provide important information regarding interactions at biointerfaces.[72] For example, the interaction forces between biologically relevant molecules and biomaterials used for implants can be obtained. Furthermore, with this information at hand, it may be possible to design biomaterial surfaces for specific needs.[73]

1.6. Surface modification and characterization

Surface modification is a process by which surfaces of known chemistry and physical properties can be prepared. Recent advances in medicine and tissue engineering have resulted in an increase in demand for new biomaterials. A good biomaterial should be biocompatible, biodegradable (and in some cases non-degradable) and posses physical properties closely mimicking those of the target tissue.[55,74] It is a challenging task to find such properties among known synthetic materials. Consequently, research performed in the area of surface modification is continuously growing. Surface modification allows the use of a material with desired bulk properties *i.e.* hardness, stiffness, elasticity *etc.*, whose surface can be modified and customized for specific purposes: make it biocompatible, hydrophobic/hydrophilic, or change its topology. Custom biointerface modification is one way of designing state-of-the-art biomaterials, which serve a specific purpose while minimizing unfavorable characteristics.[75,76]

In the context of this thesis, modification and characterization of prepared surfaces serve two major objectives: *(i)* practicality - it is experimentally easier to analyze results if the surface is prepared knowing exactly all of the parameters used in its preparation *(ii)* experimental variables - having a range of chemically and physically different surfaces is essential to evaluate structure/function relationships.

Gold coating and thiol self-assembled monolayers (SAMs) were the methods used to modify surfaces in this project. The *N*-hydroxysuccinimide activated carboxylate group of dithiobis(succinimidyl undecanoate) (DSU) homobifunctional cross-linker is reactive towards amine nucleophiles and was used to covalently attach chitosan to AFM tips.[77] The disulfide bond of this linker allows for self-assembly on gold surfaces creating a SAM reactive towards amines (Figure 20). In order to perform single molecule experiments, it is preferable to use an AFM tip which has few chitosan strands attached to its surface. To limit the amount of chitosan strands attaching to the tip, low concentration chitosan solutions were used and dodecanethiol was added to the self-assembly solution to decrease the density of amine reactive groups on the AFM tip.

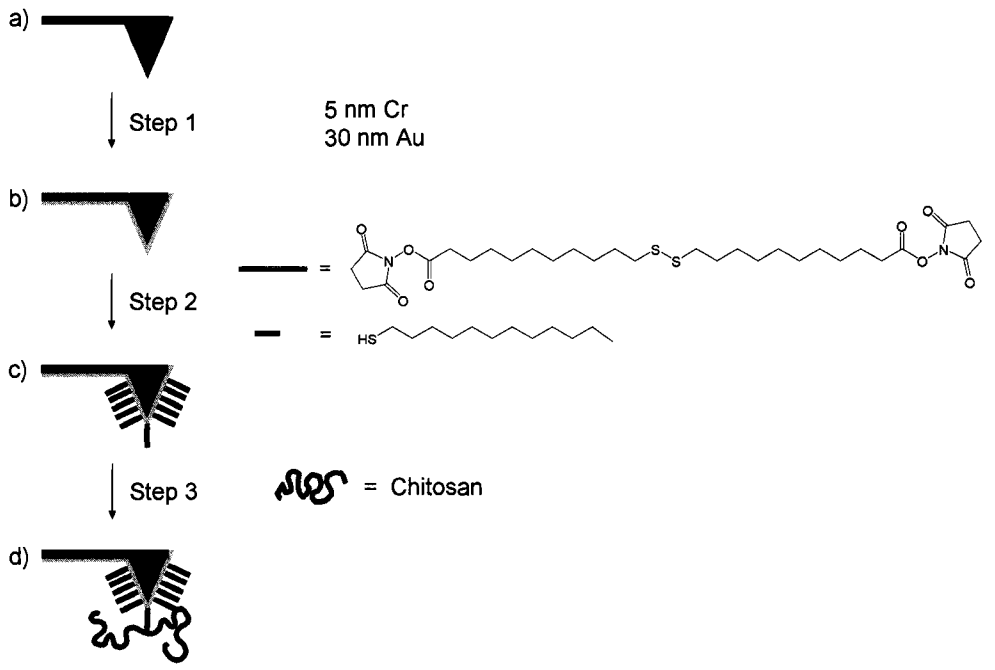

Figure 20. AFM tip functionalization. Step 1: gold coating by thermal evaporation. Step 2: self-assembly of dithiobis(succinimidyl undecanoate) diluted with dodecanethiol. Step 3: reaction of chitosan with the succinimidyl groups on the tip

Dodecanethiol, decanethiol as well as mercaptoundecanoic acid are thiol terminated molecules which also self-assemble on gold and were used to prepare surfaces with different chemistries. Surfaces that were modified and characterized in this study include mica, glass, quartz and polytetrafluoroethylene (PTFE) and various SAMs.

Glass surfaces were gold coated and used as substrates for self-assembly. Thiols with different chemical functionalities were used with the aim of creating surfaces with similar roughness but varying in chemical functionality. Mercaptoundecanoic acid was used to create hydrophilic carboxy terminated surfaces while dodecanethiol was used to obtain hydrophobic surfaces. Surfaces with SAMs of the dithiobis(succinimidyl undecanoate) were prepared for testing the covalent attachment of chitosan.

The characterization of these surfaces was performed with AFM imaging, ellipsometry, contact angle measurements and scanning electron microscopy (SEM).

AFM imaging, described in Section 1.4.2, provides an image of the surface at the nanometer scale and surface roughness can be determined.

Ellipsometry is an optical technique used to measure film thickness. The parameters used during the measurement are amplitude ratio (ψ) and phase shift (Δ). The measurement is performed by observing a change in the polarization of elliptically polarized light which is reflected or transmitted from the surface studied.[78]

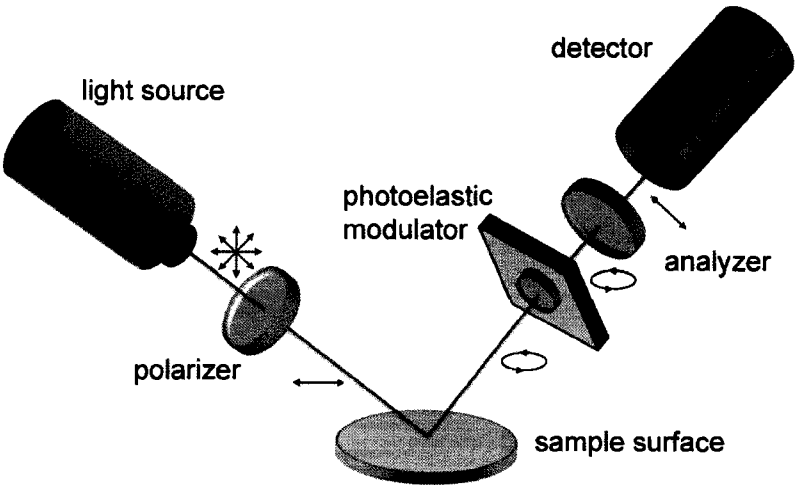

Figure 21. Schematic diagram of components in en ellipsometer

Contact angle measurements were used to determine the hydrophobicity or hydrophilicity of surfaces. In this technique, a water drop is placed on the surface of interest and the contact angle is measured. A contact angle of a drop of water on a hydrophobic surface is high (90°-180°) whereas the contact angle of a drop of water on a hydrophilic surface is low (0°-90°).

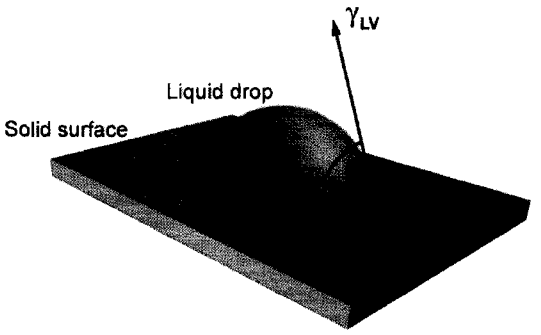

Figure 22. Contact angle measurement where γ_{LV} is the interfacial energy of the liquid-vapor boundary, γ_{SL} is the interfacial energy of the solid-liquid boundary, γ_{SV} is the interfacial energy of the solid-vapor boundary and θ is the contact angle

Scanning Electron Microscopy (SEM) is used to visualize material with nanometer resolution. Because the wavelength of electrons is orders of magnitude smaller than visible light, such high resolution is possible. SEM operates similarly to a microscope, but uses electrons instead of visible light to study the sample. This requires magnetic lenses to deflect and condense electrons.

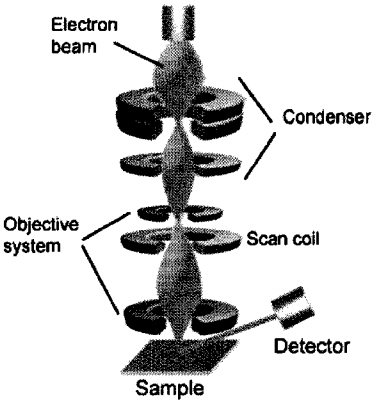

Figure 23. Scanning electron microscope

Monochromatic energetic electrons are generated at variable voltages raging from 0.5 to 20 kV by a LB_6 crystal. The electrons are accelerated into a narrow beam by an

electron gun under high vacuum (10^{-6} Torr). The electrons are then collimated into a stream, which is focused to a small, thin, coherent beam by the use of condenser lenses, a scanning coil and the objective system coils. The electron source is used to scan the sample in a raster-scan fashion. Each point being hit by electrons emits secondary electrons. The height of a surface feature, as well as its tilt angle, both co-determine the number of generated secondary electrons. The detector, which is based on a scintillator, is positioned at an angle to detect the scattered secondary electrons. The more secondary electrons are produced, the brighter the area appears in the scan. The contrast obtained represents the surface structure. The image obtained can be viewed as a 3D grayscale image, where the brightness of the area observed is a qualitative representation of feature heights. Lower areas are less accessible to the electrons and appear darker, while the opposite is observed for higher areas. SEM samples can be imaged directly if they are conducting. However, for non-conductive samples a metal layer of a few nanometers over the sample is required.[79]

In this study the main technique used to probe the single molecule properties of chitosan is AFM-based single molecule force spectroscopy. Chapter 2 of this thesis will describe the tools required for studying the interaction of chitosan molecules with biologically relevant surfaces which will be presented and discussed in Chapter 3.

Chapter 2. Experimental

2.1. Materials and methods

Chitosan samples with degrees of deacetylation (DDA) of 72, 92 and 98% with average molecular weights of 220, 200 and 110 kDa, respectively, were generously provided by Dr. M. Buschmann (Département de génie chimique, École Polytechnique de Montréal). Glacial acetic acid, hydrochloric acid, tetrahydrofuran (THF), isopropanol, dodecanethiol, decanethiol, octadecanethiol, phospahate buffered saline (PBS), acetate buffer (acetic acid and sodium acetate) were purchased from Sigma-Aldrich (Canada Ltd.) or Fisher Scientific (Canada). Dithiobis(succinimidyl undecanoate) (DSU) linker was kindly synthesized by Dr. V. Toadler who was supported by the FQRNT multi-university Centre for Self-Assembled Chemical Structures (CSACS). Deionized water was used for all solution preparations.

Hellmanex (Sigma-Aldrich; Canada Ltd.) was used to clean glass and quartz surfaces. Chromium pellets 57 x 3.2 mm (Ted Pella Inc.; USA) and gold 1g bullions 999.9 purity (Istanbul Gold Refinery; Turkey) were used for gold coating of AFM probes and glass surfaces. Surfaces used for the experiments include quartz (Concordia University Glass Blowing Facilities), glass microscope slides (Bio Nuclear Diagnostics Inc., Canada), muscovite mica (Ted Pella Inc.; USA) and PTFE (TEX-O-LON; USA, generously provided by Dr. M. Tabrizian (Department of Biomedical Engineering, McGill University))

AFM imaging was performed with a Digital Instruments' Nanoscope IIIa equipped with a fluid cell (Santa Barbara. USA) operating with NanoScope version 6.13r software. Single molecule force experiments were performed with an Asylum Research MFP-1D (USA) operating with IgorPro version 4.0.9.0 software.

Ellipsometry measurements were performed using an I-Elli2000 (Nanofilm Technologie GmbH, Göttingen, Germany) equipped with a 50 mW Nd:YAG laser (λ = 532 nm). All experiments were performed using a 20x magnification with a lateral resolution of 1 μm, an incidence angle of 70.00° and a laser output of 2% with the compensator set to 45.00°. To determine the optical thickness of the monolayer at the air-solid interface, the following two-box optical model was used: gold as substrate (n=0.5176, k=2.1005) and a generic organic film as the surface layer (n=1.5, k=0). The reported thickness is an average of 10 measurements taken at the same location on the same film and is consistent for multiple samples.

A UV-ozone oven (UVO-Cleaner, Model No. 342, Jelight Company Inc, USA) was used for treating AFM tips and gold-coated surfaces. Gold-coating was performed with a Polaron E 6300 Bench Top Thermal Evaporator equipped with a Cressington crystal balance thickness monitor (USA).

Contact angle measurements were performed on SAMs of DSU linker, mercaptoundecanoic acid and octadecanethiol with a profile analysis tensiometer (PAT-1D, Sinterface, Germany).

Silicon nitride triangular Microlever Probes MLCT-AUNM and silicon nitride NP-20 probes, used in single molecule force spectroscopy experiments and AFM imaging, respectively, were purchased from Veeco Probes, Santa Barbara, CA, USA.

Analysis of the SMFS results was performed using IGOR Pro version 5.0.4.8 software. Histograms were prepared using OriginPro 7.5 SR v7.5885 software.

The SEM experiments were carried out on a high resolution Hitachi S-4700 FE-SEM at the Facilities for Electron Microscopy Research (FEMR) at McGill University.

2.2. Chitosan preparation

Chitosan stock solution (concentration of 3.6 gL^{-1}) was prepared by dissolving 3.6 mg of chitosan powder in 1 mL of sodium acetate buffer (pH 3.9). To allow chitosan powder to hydrate and dissolve, the solution was stirred overnight to yield a viscous transparent solution. Lower concentration chitosan solutions were prepared by serial dilution of the stock solution either with sodium acetate buffer at pH 4.5-5.5 (chitosan solutions used for AFM imaging and single molecule force spectroscopy (SMFS) experiments) or 0.01 M PBS buffer at pH 7.6 (chitosan solutions used for the reaction of chitosan with the DSU self assembled monolayer on gold coated AFM tips).

Chitosan samples with DDAs of 98 and 72% and concentrations of 0.2 gL^{-1} and 0.05 gL^{-1} were used for AFM imaging. Chitosan samples with DDAs of 98, 92 and 72% and concentrations ranging between 0.25 gL^{-1} and 0.0007 gL^{-1} were used for SMFS experiments. Higher chitosan concentrations (0.25 gL^{-1}) were used for experiments where chitosan was deposited on surfaces and an unmodified AFM tip was used for probing. Lower end chitosan solution concentrations (0.0007 gL^{-1}) were used for experiments where chitosan was covalently attached to AFM tips. Chitosan with a DDA of 72% was used for initial SMFS experiments on mica and glass surfaces. Chitosan solutions with DDAs of 92 and 98% were used in the experiments where AFM tips were covalently modified with chitosan.

2.3. AFM imaging of chitosan

AFM imaging of chitosan was performed on mica under liquid conditions. A drop (*ca.* 35 μL) of dilute chitosan solution (concentration of 0.2 gL^{-1} and 0.05 gL^{-1}) was deposited on freshly cleaved mica. After 1 minute of adsorption, excess chitosan was rinsed off with sodium acetate buffer at pH 4.5-5.5. AFM imaging of the mica surface with chitosan was performed using silicon nitride triangular probes (NP-20) placed in a glass liquid cell. All of the images were obtained in intermittent contact mode (Tapping mode) in sodium acetate buffer at pH 4.5-5.5. Chitosan samples were raster scanned until images with single chitosan strands were obtained. A fresh AFM tip was used for each new surface/sample scanned. Images were flattened to remove background slope.

2.4. Probe preparation

Silicon nitride MLCT-AUNM AFM tips were used for single molecule force spectroscopy experiments and silicon nitride NP-20 AFM tips were used for AFM imaging. Prior to SMFS experiments, AFM tips were treated in the UV-ozone oven for 30 min to remove any organic contaminations that might be present from the GEL PAK® adhesive in the tip storage container.[80]

Gold-coated silicon nitride MLCT-AUNM AFM tips were prepared by evaporating a 5 nm layer of chromium followed by a 30 nm layer of gold. The layer thickness was determined with a quartz crystal thickness monitor. Gold-coated probes were chemically modified by the self-assembly of DSU linker diluted with dodecanethiol at a ratio of 1:150. The low ratio of the DSU linker to dodecanthiol was used to reduce the possible number of attachment points for chitosan. The goal was to obtain an AFM tip

with a few covalently attached chitosan strands. The self-assembly solution of DSU linker diluted with dodecanethiol was prepared in THF with an overall concentration of 1 mM. The gold coated probes were placed in the UV-ozone oven for 20 min prior to self-assembly. The probes were left undisturbed in the self-assembly solution for 24-48 hours. Each tip was taken out of the self-assembly solution and rinsed in three consecutive beakers of fresh THF. The tips were dried on a KimWipe and placed in a custom made Teflon tip holder which was then suspended in a solution of chitosan in PBS buffer for 30 min. The reaction solution was composed of 12 mL of 0.01M PBS (pH 7.6) and 50 μL of chitosan (DDA 92%, concentration of 0.25 gL^{-1}, pH 7.6). The tip holder was then transferred to a beaker which contained acetate buffer (pH 4.5) with the goal of solvating any chitosan molecules which were not covalently attached to the tip. The buffer was changed daily for 3 days. The tips were removed from the tip holder, placed in a closed container with acetate buffer and stored at 5°C. Tips were stored for no longer than one week to limit buffer contamination.

2.5. Surface preparation and characterization

Surfaces used for single molecule force spectroscopy experiments must be exceptionally clean of any contamination due to the sensitivity of the technique. To test the efficacy of the cleaning procedures, comparisons were made by acquiring force curves with a new UV-ozone treated silicon nitride tip on both 'as received' and cleaned surfaces. Surfaces were considered clean if no desorption events were observed in the force curves. Besides the cleaning procedures the following sections include the procedures for self-assembly of monolayers on surfaces and their qualitative characterization.

2.5.1. Microscope slides, quartz and mica

All the microscope glass slides and quartz used for the SMFS experiments were cleaned with acetone to remove any grease and then sonicated for 30 min in 2% Hellmanex solution at 50 °C. The slides were rinsed 5 times with distilled water. After rinsing, the slides were sonicated again, this time in 10% isopropanol to remove any residual surfactant remaining on the surface. The slides were then rinsed again with distilled water (5x) and stored in clean water until used. Slides were stored for no longer than 5 days. Prior to SMFS experiments, the slides were removed from the water and dried in an oven.

Freshly cleaved muscovite mica was used for AFM imaging and SMFS desorption experiments.

2.5.2. Gold-coating of glass slides

Gold-coated glass slides were prepared at the same time as the gold-coated AFM tips by thermal evaporation of 5 nm of chromium followed by 30 nm of gold. Prior to gold-coating, glass microscope slides were cut into 1 cm^2 pieces using a diamond tip pen cutter and then cleaned in the same manner as described for the glass slides in Section 2.5.1. The slides that were not used immediately after preparation were stored in a covered Petri dish. Before using the gold-coated slides for self-assembly, the slides were treated in the UV-ozone oven for 30 min.

2.5.3. Self-assembled monolayers (SAMs) on gold

Chemically modified surfaces were prepared by immersing clean gold-coated surfaces in 1 mM self-assembly solutions of DSU linker or a mixture of DSU linker:dodecanethiol with a ratio of 1:1000 and total concentration of 1mM in THF. The gold-coated surfaces were treated in a UV-ozone oven for 30 minutes prior to the self-assembly which was carried out overnight. Once prepared, the surfaces were rinsed (5 x 5 mL) with fresh THF and dried in a stream of nitrogen. Mercaptoundecanoic acid SAM surfaces were prepared in a similar fashion. The self-assembly was performed overnight in ethanol. Once prepared, the surfaces were rinsed with ethanol (5 x 5 mL) and dried in a stream of nitrogen. The surfaces were prepared immediately prior to SMFS experiments.

2.5.4. Polytetrafluoroethylene (PTFE)

The PTFE polymer surface (approx 1 cm^2) was stirred in 1M nitric acid overnight, followed by rinsing in deionized water to remove any nitric acid (50 mL of fresh water, 3x) and stirred overnight in acetate buffer at pH 5.0. The surface was rinsed with deionized water and dried in a stream of nitrogen.

2.6. SMFS experiments of chitosan

Spring constants of the cantilevers used for SMFS experiments were determined by: (*i*) calibrating the Inverse Optical Lever Sensitivity (InvOLS) of the cantilever and (*ii*) acquiring the thermal Power Spectral Density (PSD) graph of the cantilever. InvOLS is acquired by pressing the cantilever into a hard surface and calculating the slope of the force curve recorded. The InvOLS is the sensitivity of the cantilever-detector combination and is reported in nm V^{-1} (*i.e.* the value is detected by the photodetector

when the cantilever is deflected by a certain distance, x). The photodetector reports the cantilever deflection in volts, therefore, these values must be multiplied by the InvOLS to obtain the accurate deflection of the cantilever in nm. The PSD is recorded when the cantilever is far away from the surface and vibrates due to thermal motion; this PSD data shows the amplitude of the signal versus the frequency. The recorded data is fitted with a simple harmonic oscillator function, the area under this fit is determined and the spring constant is calculated.

All experiments were performed at a 0.5 Hz scan rate, with a sampling rate of 20000 points per second and a digital filter bandwidth of 10 kHz on the incoming deflection data.

2.6.1. AFM tip interactions with various surfaces

To eliminate capillary forces which would overwhelm the small forces of interest to this study,[81] experiments were performed under complete liquid immersion conditions. A drop of buffer was deposited on both the surface and the AFM tip. When the two surfaces were brought into contact, a meniscus formed between the tip and the surface providing a liquid environment for the experiment. Both, unmodified and chitosan-modified AFM tips were approached to and retracted from the surface until force curves showing interactions were observed. Multiple areas of the surface were investigated in order to either: (*i*) locate and probe upon randomly dispersed chitosan strands or (*ii*) probe different areas of the bare surface with the chitosan-modified AFM tip. On average, 200 curves were collected and saved in each area of the surface. When force curves indicating desorption events are obtained (*i.e.* single point desorption peaks with baseline prior to the single point desorption event or constant force desorption plateaus)

force curves are collected until the interaction is lost. Many conditions were taken into consideration to successfully carry out SMFS experiments on single polymer strands of chitosan. First, AFM imaging was performed to determine the appropriate chitosan concentration to obtain isolated strands on surfaces. SMFS experiments were carried out to evaluate chitosan adhesion to various surfaces. To ensure that only the chitosan-surface interaction was measured (as opposed to the chitosan-tip interaction) chitosan was covalently bound to the AFM tip. Although the chitosan was probed using both unmodified and modified AFM tips, the chitosan tip modification technique proved most useful to probe different surfaces and to obtain both quantitative and qualitative results for the adhesion properties of chitosan. The chitosan-modified tips also provided the best data to extract the mechanical properties of chitosan using curve fitting techniques.

Generally, the experiments presented can be summarized as follows. An *unmodified* or *chitosan-modified* AFM tip was approached to a surface and the interaction with this surface was recorded in the form of force curves. A force curve is composed of an approach trace and a retraction trace. In this work, only the retraction curves are considered. The types of force curves observed contained: (*i*) no interactions, (*ii*) single desorption peaks close to the surface (*i.e.* no baseline before the peak), (*iii*) single desorption peaks far from the surface (*i.e.* baseline or plateau before the peak), (*iv*) constant force desorption plateaus or (*v*) some combination of the above mentioned features. Force curves without any interactions or containing only single point desorption peaks close to the surface were not included in the histogram analysis; these corresponded to non-specific tip-surface interactions. For experiments performed with

unmodified tips, a dilute concentration of chitosan was deposited on the surface to allow single molecule adsorption, in order for single molecules to be probed. These experiments are expected to yield a low number of interaction force curves because the tip is unmodified and the chitosan surface coverage is low. Therefore, the probability of the tip 'finding' a chitosan molecule is low and this gives rise to a low yield of successful pulling events. In experiments where chitosan-modified tips were used, the number of force curves with interaction events is higher because the tip is covalently modified with chitosan molecules.

Constant force desorption plateaus were analyzed with respect to both their desorption forces (*i.e.* plateau height) and plateau lengths. The constant force desorption results were compiled in histograms showing the number of events and their magnitude. Force curves containing single point desorption peaks were analyzed with respect to their peak heights. Materials with varying surface free energies were probed to compare the adhesive properties of chitosan to these surfaces. Surface free energy is a measure of surface characteristics and interfacial interactions such as adsorption. Surface free energy can be used to evaluate the adhesive properties of a surface to another material, in this case chitosan.

2.6.2. Analysis of SMFS results

A procedure using IgorPro software was written to allow the analysis of force curves collected during experiments. To perform the analysis of single point desorption peaks, the average value between cursors on horizontal regions of the force curves were obtained and compared. The heights of constant force plateaus were obtained by

calculating the average value between the cursors placed on the baseline of the retraction curve and the average value between cursors placed on the plateau. The difference between these two values was the height of the plateau. In cases where there was ambiguity (*i.e.* if it was not clear if two plateaus of different heights were observed or if it was one plateau with noise) a t-test was performed on the data sets to determine if they are statistically different (*i.e.* two different plateaus) or not (*i.e.* the same plateau with noise) (Equation 6).[82]

$$t = \frac{\bar{X}_1 - \bar{X}_2}{\sqrt{\frac{(N_1 - 1)SD_1^2 + (N_2 - 1)SD_2^2}{N_1 + N_2 - 2}}} \sqrt{\frac{N_1 N_2}{N_1 + N_2}}$$

Equation 6. t-test equation where $\bar{X}$ is the average value of a population of points (*ie.* one plateau equals one population of points), SD is the standard deviation of a given population and N is the number of points in a population

When $N \geq 800$, $N_1 \approx N_2$ and $SD_1 \approx SD_2$, the t-test equation was rearranged and simplified into Equation 7 in order to estimate the difference between the averages needed to assume their distinction.

$$\bar{X}_1 - \bar{X}_2 \geq \frac{3}{20} SD$$

Equation 7. Rearrangement of the t-test equation

The area under a constant force plateau was calculated by multiplying the last plateau height of a force curve by its length to obtain the energy of desorption of the given chitosan strand. This energy was divided by the number of glucosamine residues (*i.e.* the length of the plateau divided by the length of one glucosamine residue: 0.52 nm)[18] to extract the single glucosamine residue energy of desorption.[52]

Force curves with single point desorption peaks preceded by a baseline were used for fitting with the freely jointed chain (FJC) model. The curves were offset to zero force and distance and rotated from their original graph presentation to obtain positive force values essential for fitting. Multi pass box (500 points) smoothing of the force curves was performed prior to fitting. Cursors were placed at the beginning of the extension of the polymer (*i.e.* where the baseline starts increasing) and in the upper part of the extension of the peak (*i.e.* half-way to the rupture point). Cursors were repositioned slightly until a good fit was obtained (*i.e.* the fit was overlapping with the baseline and the initial extension of the polymer chain). Values of contour length and Kuhn length were obtained from the curve fits.

Chapter 3. Results and discussion

Many experimental surveys have been performed on polymers in bulk, with the aim of determining their unique characteristics, and to improve the understanding of their behavior under various conditions.[83] In this study, SMFS is the polymer characterization tool used to investigate the properties of the chitosan polymer at the molecular level. Parameters such as contour length (l_C), Kuhn length (l_K), unfolding forces and surface specific desorption forces are determined from single molecule measurements. Polysaccharides, such as dextran, amylose, pullulan, pectin, cellulose, and xanthan have been previously studied by SMFS and their single molecule properties have been obtained.[3,61,84] This chapter describes the results of single molecule characterization of chitosan. Apart from this work, to our knowledge, there are no SMFS studies on chitosan reported in the literature.

Chitosan behaves as a polyelectrolyte when dissolved in buffers below its pKa of 6.5[15]. The pendant amino groups can be protonated in aqueous solution giving rise to a polycation with positively charged amino groups ($-NH_3^+$) along the polymer chain. The experimental results of chitosan interactions with different surfaces are expected to be dependant on the polyelectrolyte properties of this polymer. The adhesion force of chitosan to different surfaces has therefore been studied: specifically, mica, glass, quartz, self-assembled monolayers and polytetrafluoroethylene (PTFE) were investigated. Mechanical properties were also extracted from the SMFS results and values for the

Kuhn length and contour length were obtained by using the freely-jointed chain (FJC) model.

The experimental results discussed herein are AFM imaging, probe preparation, characterization and adhesion properties of chitosan: (*i*) unmodified tip interactions with chitosan strands deposited either on mica or glass slides, (*ii*) chitosan-modified tip interactions with quartz, (*iii*) chitosan-modified tip interactions with self-assembled monolayers (SAMs) of dithiobis(succinimidyl undecanoate) (DSU), (*iv*) chitosan-modified tip interactions with SAMs of mercaptoundecanoic acid:dodecanethiol and (*v*) chitosan-modified tip interactions with polytetrafluoroethylene (PTFE). In addition, the desorption energy of chitosan and the determination of its mechanical constants is reported.

3.1. AFM imaging

To perform single molecule experiments using the SMFS technique, an AFM tip has to ideally make contact with a single polymer strand. The surface area of an AFM tip apex is approximately 4000 nm^2 and can thus adsorb multiple chitosan strands at once. When depositing chitosan onto a surface, low concentration solutions must be used to assure that the polymer strands are well dispersed and that they do not interact with each other.

Determination of optimal chitosan surface coverage for single molecule experiments was confirmed by AFM imaging of drop cast chitosan solutions on mica. A drop of 0.18 gL^{-1} solution shows chitosan aggregates with very few isolated polymer strands (Figure 24).

Figure 24. Tapping mode AFM image of chitosan (0.18 gL^{-1}) on mica in sodium acetate buffer at pH 5.1

This solution was diluted to a concentration of 0.05 gL^{-1}, deposited on mica and imaged. The resulting images showed sparsely dispersed chitosan strands (Figure 25). Single strands as well as entangled bundles of chitosan were visible on the mica surface. A low surface coverage, essential for performing single molecule force experiments, was obtained and solutions with concentrations in the same order of magnitude were used for subsequent experiments.

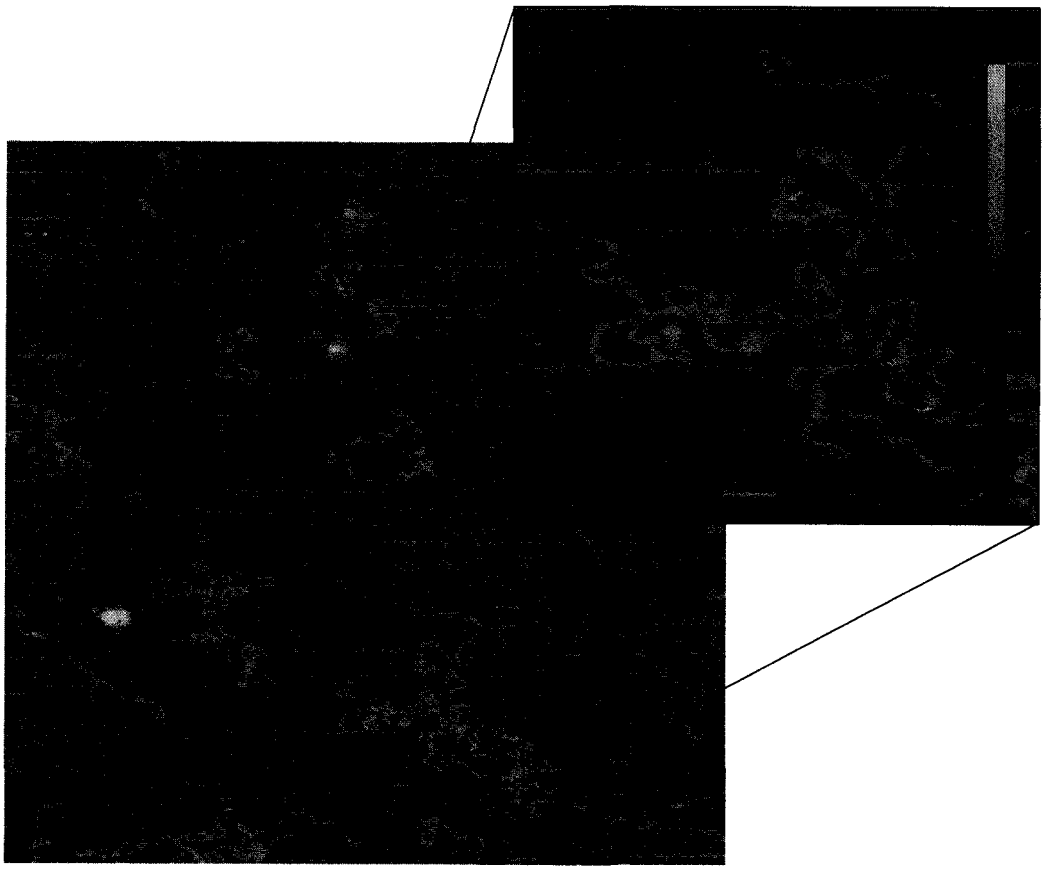

Figure 25. Tapping mode AFM image of chitosan (0.05 gL^{-1}) on mica in sodium acetate buffer at pH 5.1

AFM imaging also provided useful information about chitosan adhesion to mica and the AFM tip. Chitosan readily adhered to the silicon nitride tip used during imaging as exemplified by the great difficulties encountered during imaging. Obtaining high resolution images was challenging because of the ease of tip contamination with chitosan. High resolution images were obtained when the surface was raster scanned with a new tip. Image quality typically degraded as scanning time progressed. On the other hand, the adhesiveness of chitosan to mica is exemplified in consecutive scans shown in Figure 26. Little rearrangement of chitosan strands was observed which is essential for obtaining meaningful images and also provides information regarding chitosan's favorable interactions with mica. This adhesion can be explained by the favorable interaction

between the protonated amine groups of the chitosan strands with the negatively charged mica surface at pH 5.1.[85]

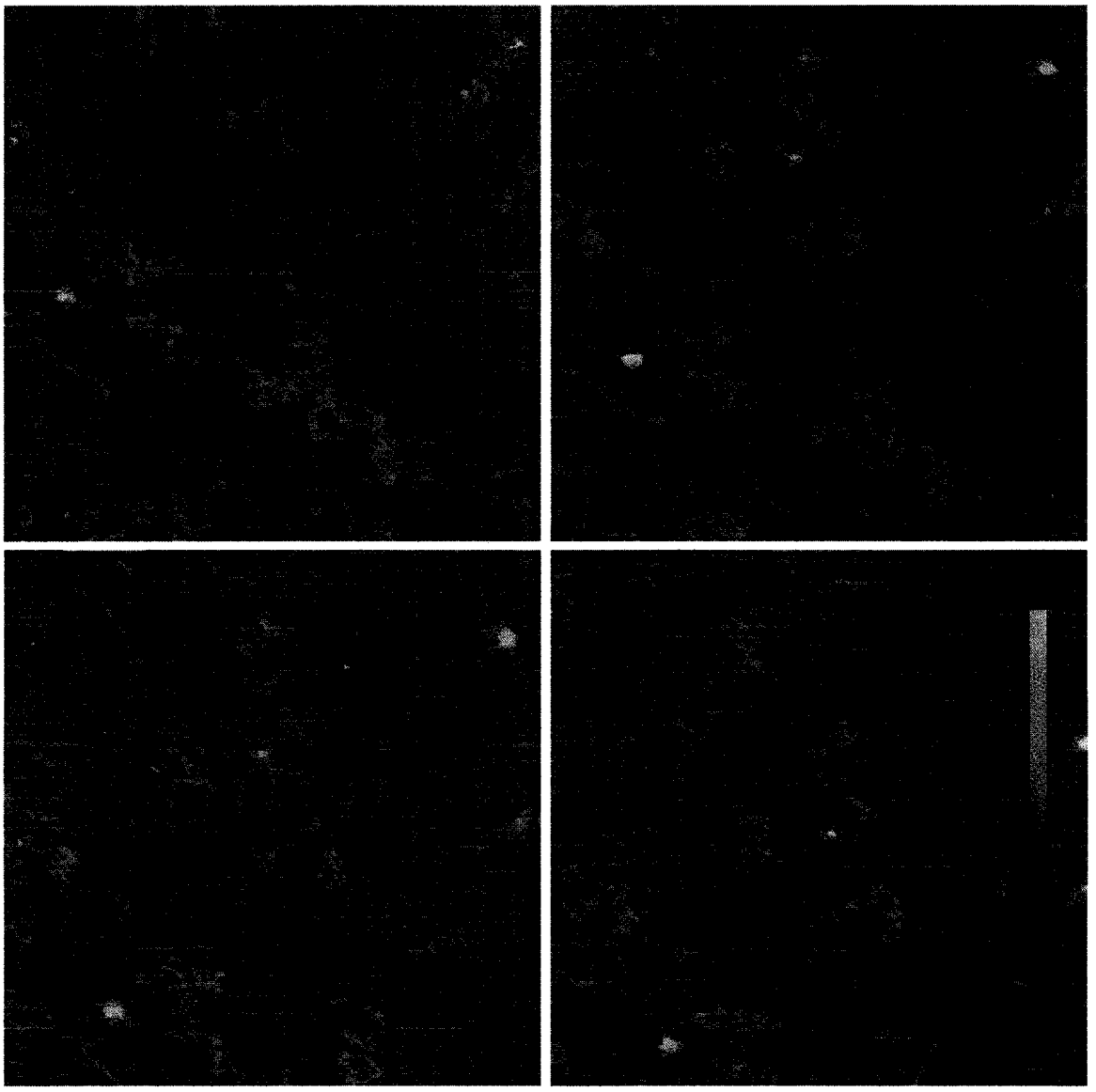

Figure 26. Consecutive tapping mode AFM images of chitosan (0.05 gL^{-1}) on mica in sodium acetate buffer at pH. 5.1: a) scan direction downwards, b) scan direction upwards, c) scan direction downwards, d) scan direction upwards. The black circle present in each image highlights the minimal rearrangement of chitosan strands during imaging.

Quantitative information such as molecular height and width can be easily extracted from a high resolution AFM image.[86] Molecular height values are more accurate than the molecular width values due to the resolution limiting factor associated with the size of the

tip.[87] The apparent size of lateral measurements is increased by the radius of curvature of the tip apex. The larger the tip radius, the greater the error in the measurement which can be explained by the tip broadening effect (Figure 27).

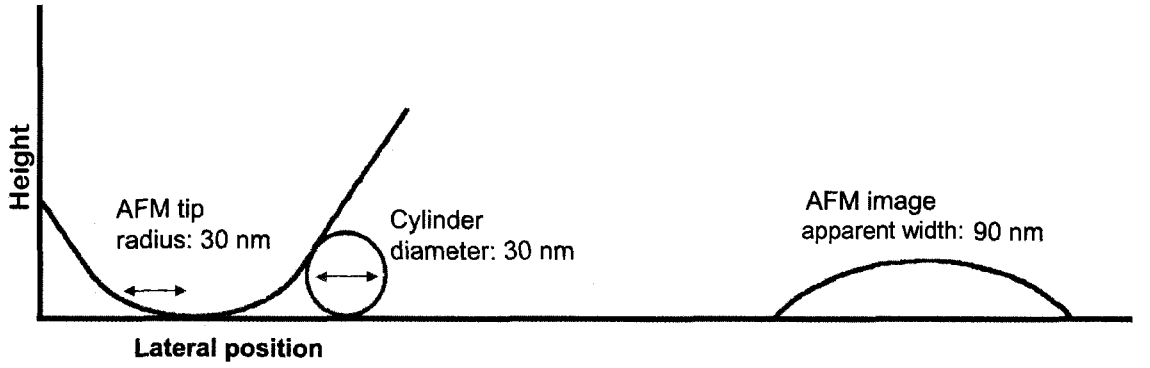

Figure 27. Broadening of features by an AFM tip (image adapted from ref. 87)

A chitosan strand cross section is shown in Figure 28. The average value of molecular height is 0.45 ± 0.04 nm. This value agrees with those reported previously for other polysaccharides.[86] The average molecular width of the chitosan strand is 5 ± 1 nm.

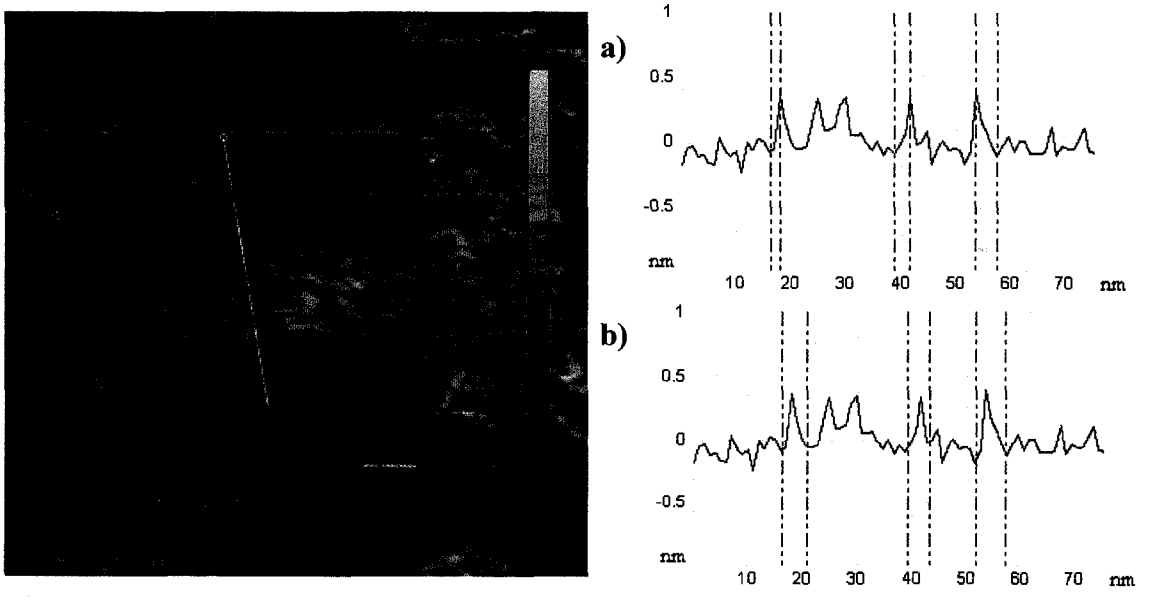

Figure 28. Cross sections of chitosan strands heights (a) and widths (b)

This value is smaller than the average values reported in the literature where some of the molecular widths of polysaccharides are an order of magnitude larger. The reason for this improved width measurement may be the heightened lateral resolution obtained when performing the AFM imaging in liquid environment, furthermore, microscopic imperfections on the tip may have provided a very sharp scanning probe (Figure 29).[88]

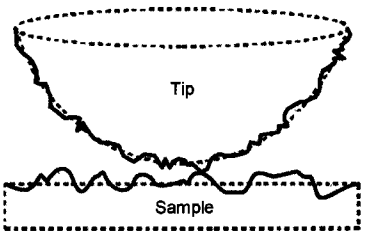

Figure 29. Schematic representation of idealized (dashed line) and real (black line) AFM tip and sample surfaces (image adapted from ref. [88])

A major concern in this SMFS study is to distinguish between desorption phenomena occurring from the surface or from the tip. In order to investigate chitosan interactions with various biologically relevant surfaces, tips covalently modified with chitosan strands were prepared.

3.2. Tip preparation

Single molecule experiments were performed following two methods: (*i*) using AFM tips as received from the manufacturer or (*ii*) covalent modification of AFM tips with chitosan. The covalent attachment of chitosan eliminates problems related to distinguishing between the desorption of chitosan from the surface or from the tip. By eliminating the latter, covalent tip modification will provide force curves that must

represent the chitosan desorbing from the surface (*ca.* hundreds of pN) or cleavage of covalent bonds (*ca.* 1-2 nN).[60]

All the tips used in the unmodified tip experiments were cleaned using a UV-ozone oven. SEM images of the silicon nitride tips are shown in Figure 30. These images show the geometry of the tip used to probe chitosan polymers and also provide a good comparison of tip quality before and after modification with gold.

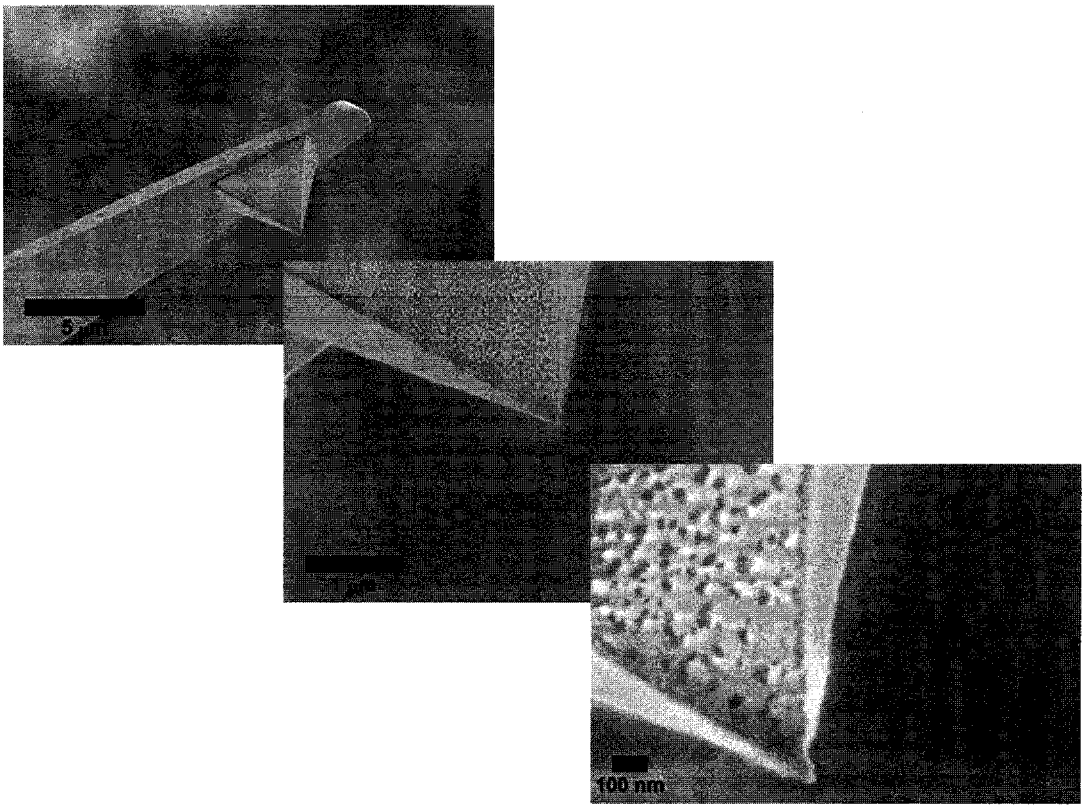

Figure 30. SEM images of an unmodified AFM tip

Covalently modified chitosan tips were prepared by self-assembly of dithiobis(succinimidyl undecanoate) (DSU) linker on gold coated silicon nitride tips and subsequent reaction with chitosan. As mentioned above, the first step towards covalent

attachment of chitosan to AFM probes was gold coating of the silicon nitride tips. The AFM probes were prepared by the deposition of a 5 nm layer of chromium followed by a 30 nm layer of gold. SEM images showing tip geometry of the AFM probes prior and subsequent to gold coating were obtained (see Figure 31 and Figure 32). The pyramidal geometry of the tip was conserved after chromium and gold deposition.

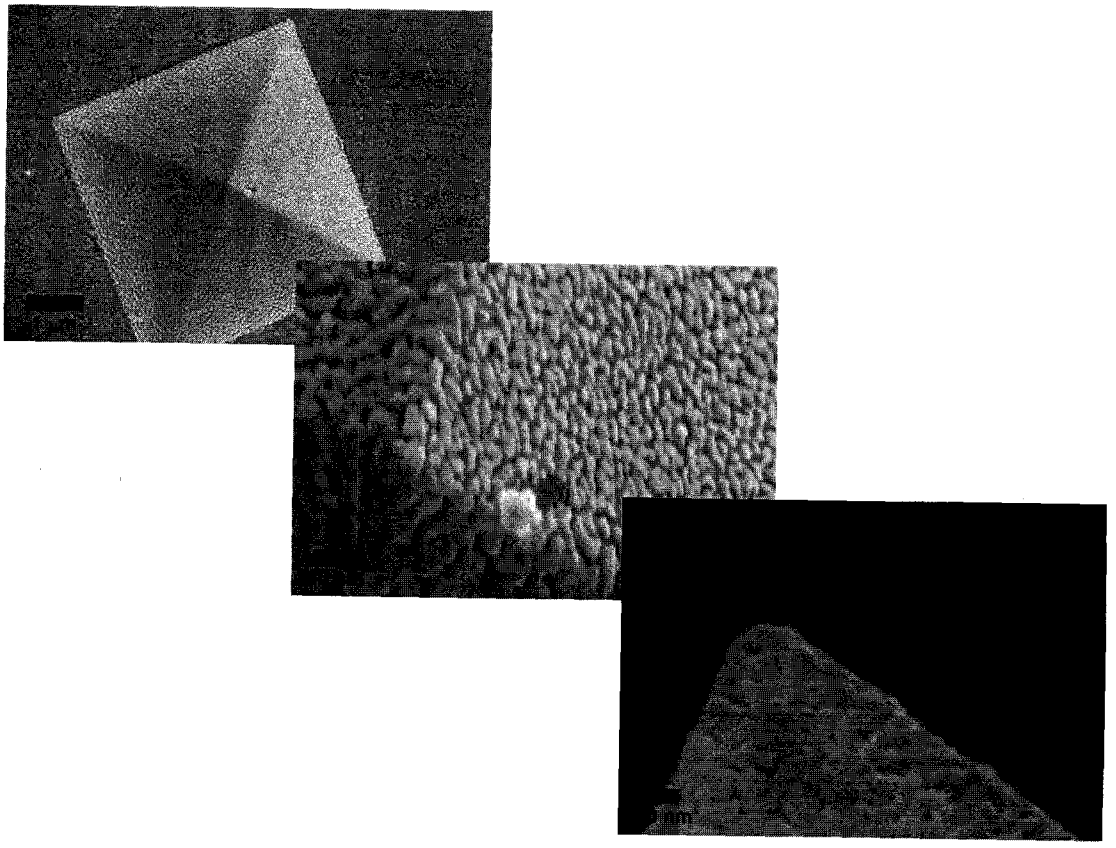

Figure 31. SEM images of a gold-coated AFM tip

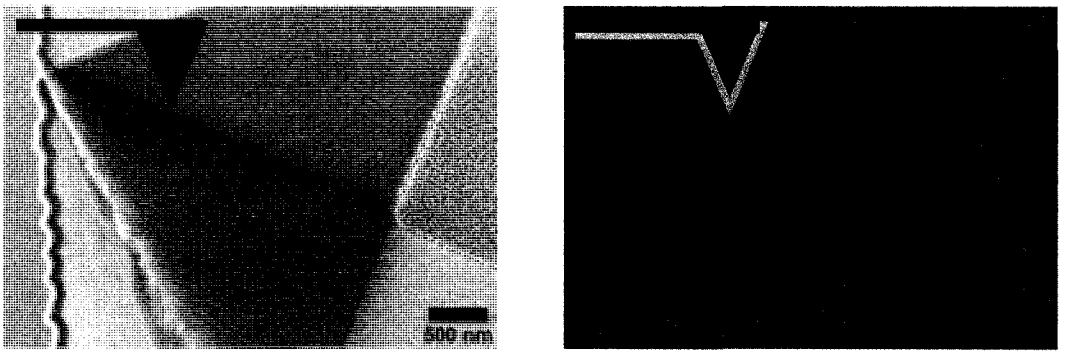

Figure 32. SEM images of the pyramidal geometry of an AFM tip prior to and following gold coating

Gold coating of the probes was followed by the self-assembly of DSU linker diluted with dodecanethiol. The amine groups of chitosan react with the succinimidyl functionality to produce an amide linkage. The low ratio of DSU to dodecanethiol molecules minimize the number of chitosan strands attached to the AFM tip by minimizing the number of chitosan attachment points.

The results from experiments performed with unmodified and chitosan-modified AFM tips as well as a comparison between the two are presented in the following sections.

3.3. Surface preparation and characterization

Contact angle measurements were performed on different self-assembled monolayers (SAMs): DSU, mercaptoundecanoic acid and octadecanethiol. The contact angles of octadecanethiol and mercaptoundecanoic acid SAMs were measured as reference surfaces to which the linker SAM surface was compared (Figure 33). The hydrophobic octadecanethiol SAM had a contact angle of 98° ± 2°. In comparison, the hydrophilic mercaptoundecanoic acid SAM had a contact angle of 27° ± 0.5°. The

chemical structure of the latter surface should be identical to the chemical structure of a fully hydrolyzed DSU SAM. The contact angle of the DSU SAM was 54° ± 1°. This value corresponds well to the literature value and is larger than the contact angle on the mercaptoundecanoic acid SAM, suggesting that the surface groups of the DSU SAM are not hydrolyzed and should therefore be reactive towards the amine groups of chitosan.[89]

Figure 33. Contact angle measurements of water on: a) octadecanethiol SAM, b) mercaptoundecanoic acid SAM and c) DSU linker SAM. The contact angles observed were: a) 98° ± 2, b) 27.0° ± 0.5 and c) 54° ± 1

Gold-coated surfaces with SAMs of DSU linker were also characterized by ellipsometry. The film thickness measured was 0.6 ± 0.1 nm, indicating the presence of linker molecules on the surface, which is necessary to perform covalent bond cleavage tests.

3.4. Adhesion properties of chitosan

3.4.1. Chitosan deposited on mica and glass probed with unmodified tips

Solution concentrations used in AFM imaging (*ca.* 0.05 gL^{-1}; Section 3.1) were used for the preparation of surfaces to perform single molecule force spectroscopy (SMFS) experiments. Both mica and glass surfaces were prepared by depositing a drop of

dilute chitosan solution, allowing adsorption for *ca.* 1 min and unbound chitosan was subsequently rinsed from the surface with excess buffer prior to SMFS. In these experiments, the surface coverage of adsorbed chitosan is required to be sub-monolayer in order to obtain force curves with single molecule events.

The mica surface was probed with an unmodified AFM tip, and most of the force curves (*ca.* 70%) did not show any desorption events. In the remaining 30% of force curves, single desorption peaks and constant force desorption plateaus were observed. Some representative force curves are shown in Figure 34.

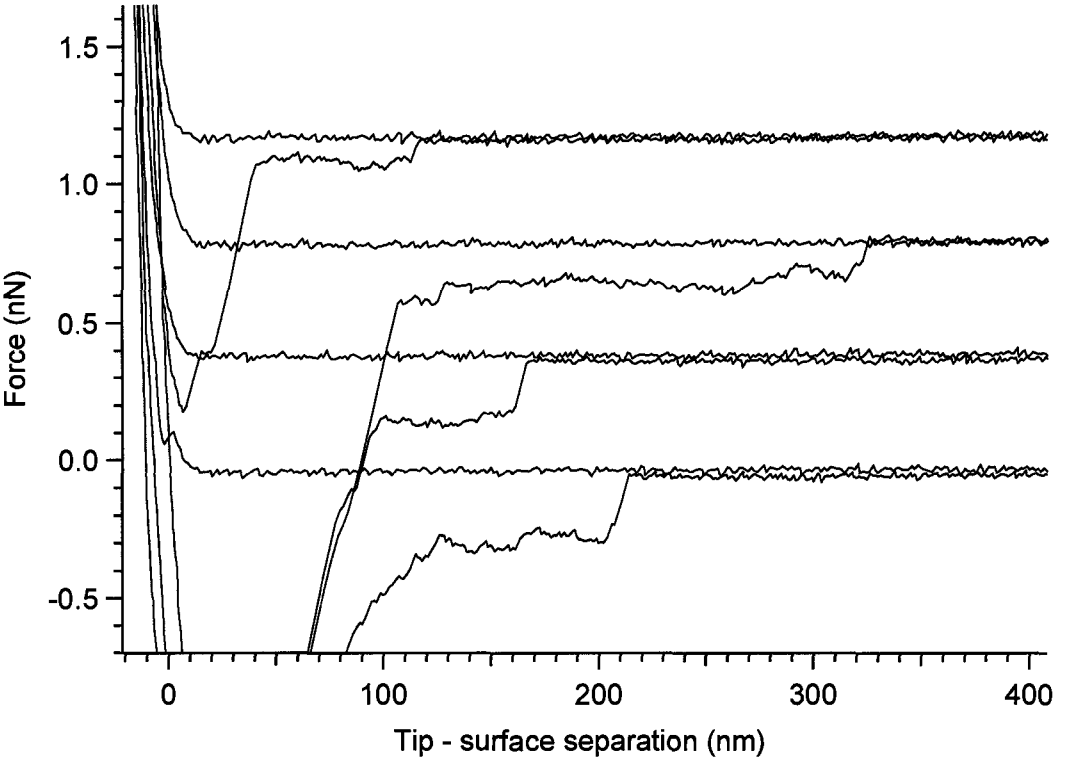

Figure 34. Typical force curves obtained by probing chitosan with an unmodified AFM tip on mica in acetate buffer at pH 5.4

Plateau features were observed in 18 of 118 force curves collected. These plateaus suggest the desorption of elongated chitosan strands uniformly spread on the mica surface. These results agree with the AFM imaging of chitosan described in Section 3.1, which showed sparsely spread chitosan strands over the entire mica surface. Figure 35 shows a schematic representation of an unmodified AFM tip interacting with chitosan on a surface. As the tip probes the surface, it can make contact with either: (*i*) an empty area of the surface which results in a force curve with no interaction force, (*ii*) a chitosan strand which adheres to the AFM tip resulting in a single point desorption peak or in a constant force plateau or (*iii*) a chitosan strand which does not interact enough with the tip to desorb from the surface, producing a force curve with an initial peak close to the surface, but no desorption features.

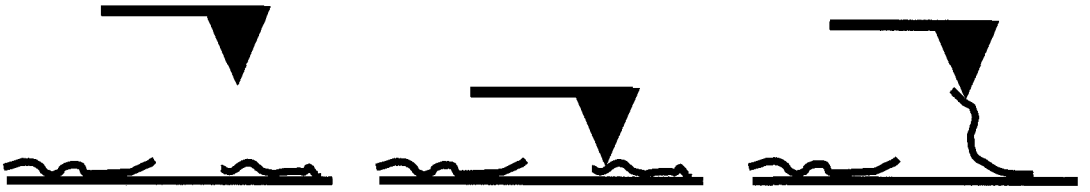

Figure 35. Schematic representation of possible unmodified tip interactions with chitosan strands on a surface

The height of a plateau is the magnitude of the adhesion force of chitosan with the mica surface. Chitosan adheres to mica with forces ranging mostly between 80 and 220 pN (Figure 36). This corresponds to the force required to desorb one or more chitosan strands from the surface.

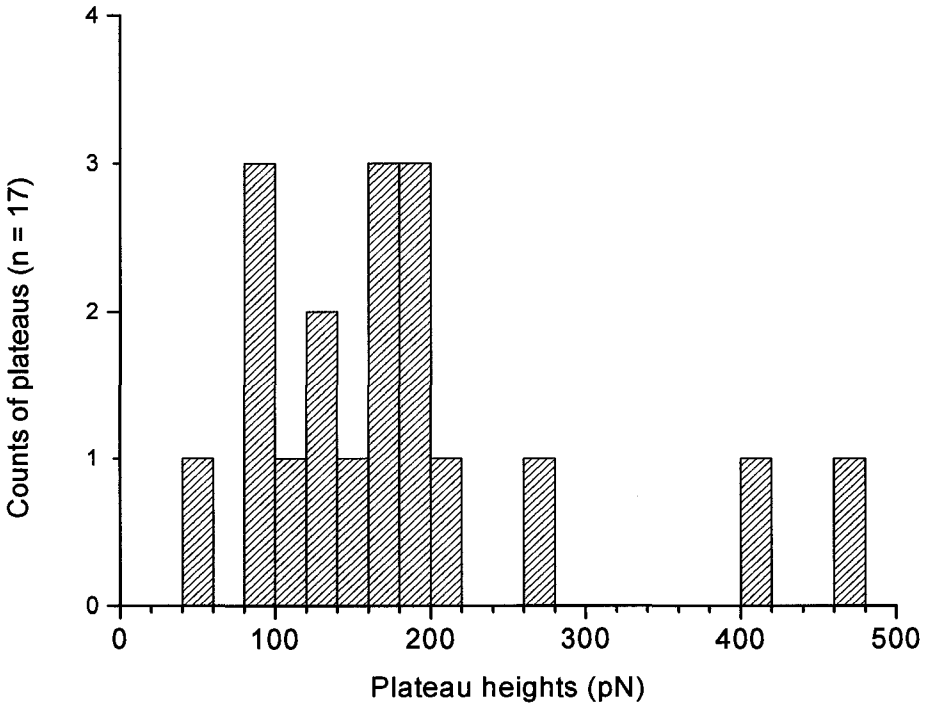

Figure 36. Plateau heights of chitosan strands desorbed from a mica surface with an unmodified AFM tip at pH 5.4

The plateau lengths range between 25 nm and 350 nm and represent the chitosan length desorbed from the surface (or from the tip). This length is not a measure of the actual polymer length but rather a measure of the distance between the sites where the chitosan strands interact with both the tip and the surface. Plateaus with multiple steps are not observed. This is likely because the probability of probing more than one evenly spread chitosan strand at the same time is very low, due to low chitosan surface coverage as shown in the AFM images in Section 3.1.

The chemical composition of muscovite mica is $KAl(SiAl)O_{10}(OH)_2$ and it can be easily cleaved along its main crystal plane yielding atomically flat surfaces. These crystal planes are ionically bonded through potassium ions. Once cleaved and exposed to aqueous solution the potassium ions are lost and the resulting surface of mica is negatively charged.[85] Adsorption of chitosan on this surface can be due to the negative surface charge on mica. In addition, the low surface roughness of mica is also expected to play a role in its interaction strength with chitosan. At pH 5.4, the amine groups of chitosan are protonated and can interact electrostatically with the negatively charged mica surface[85].

Chitosan was also deposited on glass microscope slides and an unmodified AFM tip was used to probe this surface in the same manner as reported for mica. Typical force curves representing chitosan interactions with glass are shown in Figure 37.

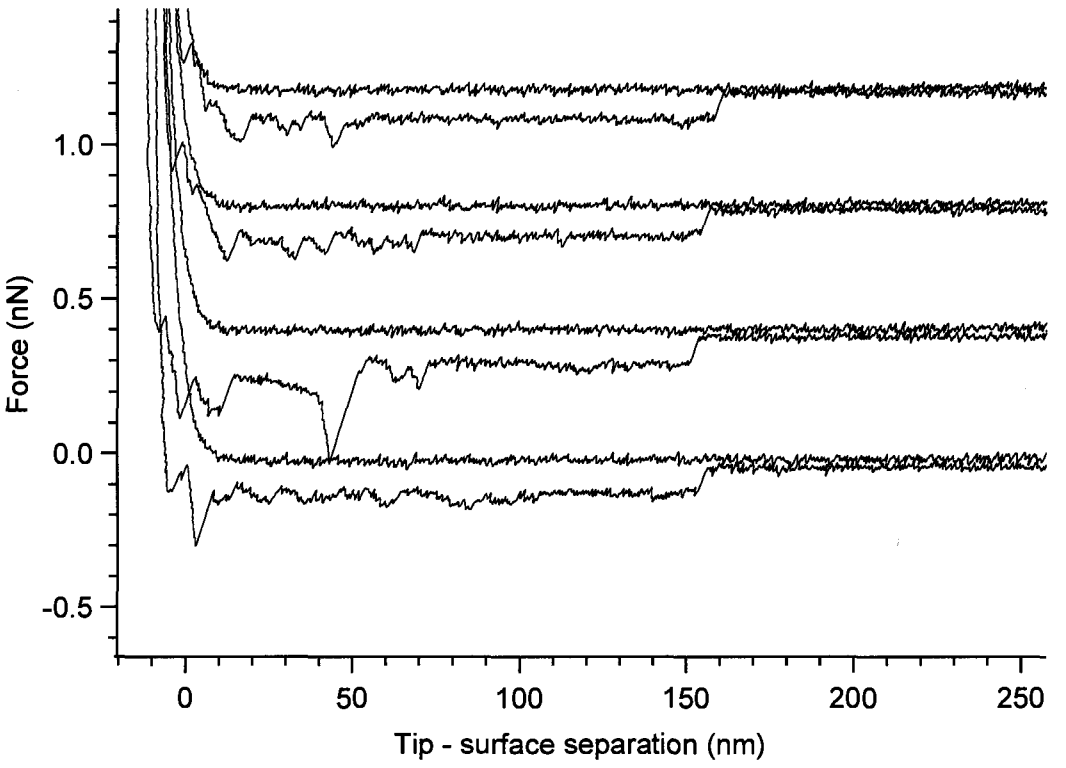

Figure 37. Typical force curves obtained by probing chitosan with an unmodified AFM tip on glass in acetate buffer at pH 5.4

Similarly to the force curves obtained on the mica surface, only a small percentage of all force curves (*ca.* 20%) have chitosan desorption features. In the few curves that did show features, plateaus were observed (Figure 38). In sequential force curves identical plateau lengths and heights, which are a signature of SMFS experiments on the same molecular strand, were observed. Repetitive plateau patterns, with regards to plateau steps and plateau lengths, have been observed previously and have also been attributed to repeatedly pulling the same molecules that are covalently attached to the AFM tip.[49]

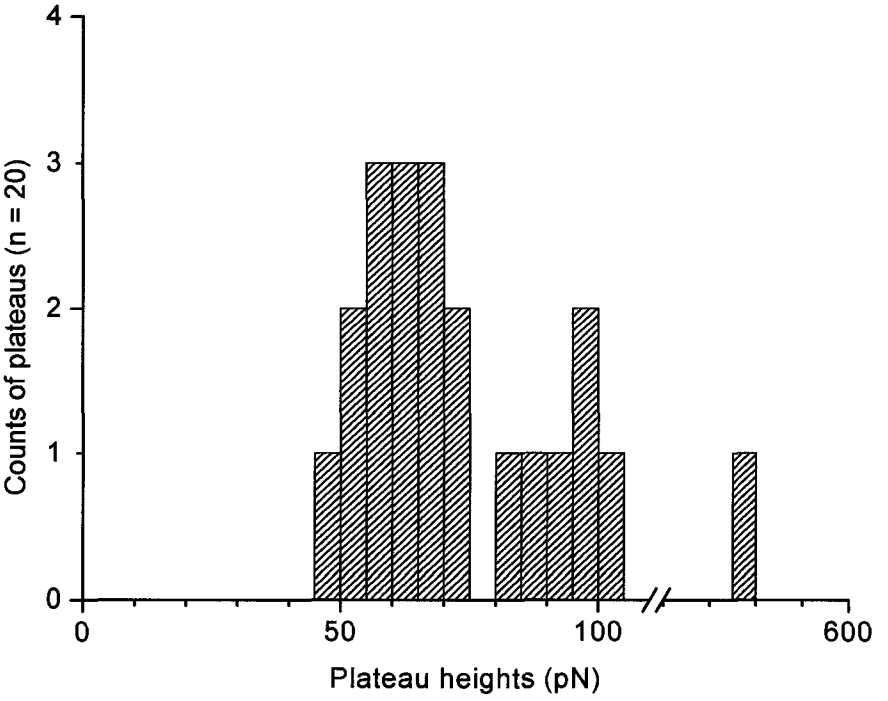

Figure 38. Plateau heights of chitosan strands desorbed from a glass surface with an unmodified AFM tip at pH 5.4

Based on the results in Figure 38 chitosan adheres to glass with forces ranging mostly between 45 and 105 pN. In comparison to the forces observed on mica, where the plateau heights ranged between 80 and 220 pN, the desorption forces of chitosan from glass were slightly lower. Glass is a noncrystalline form of quartz (SiO_2) containing varying percentages of Na_2O, CaO, MgO, Al_20_3 or other trace oxides.[90] The lower forces of chitosan adhesion can be attributed to the non-uniform distribution of surface charge on glass. The surface charge of both glass and mica in buffer (pH 5.4) is negative. The lengths of the plateaus observed on glass were between 20 nm and 160 nm with 80% of the plateaus under 80 nm. These lengths are similar to those observed on mica. The

surface coverage by chitosan stands is low on both surfaces and therefore results in few (*ca.* 20%) force curves with chitosan desorption. Constant force plateaus on glass have slightly lower magnitudes with a smaller force range. Given the number of constant force plateau data collected on both glass and mica, the results indicate similar adhesive behavior of chitosan on these surfaces.

3.4.2. Chitosan-modified tip interactions with quartz

The interaction of chitosan-modified tips with quartz is dependant on the surface charge of quartz and chitosan at a given pH. Chitosan-modified tips were prepared following the procedure described in Section 3.2. The chitosan-modified tip was approached to and retracted from the quartz surface until force curves with desorption events were observed. Typical force curves representing chitosan desorption from quartz are shown in Figure 39.

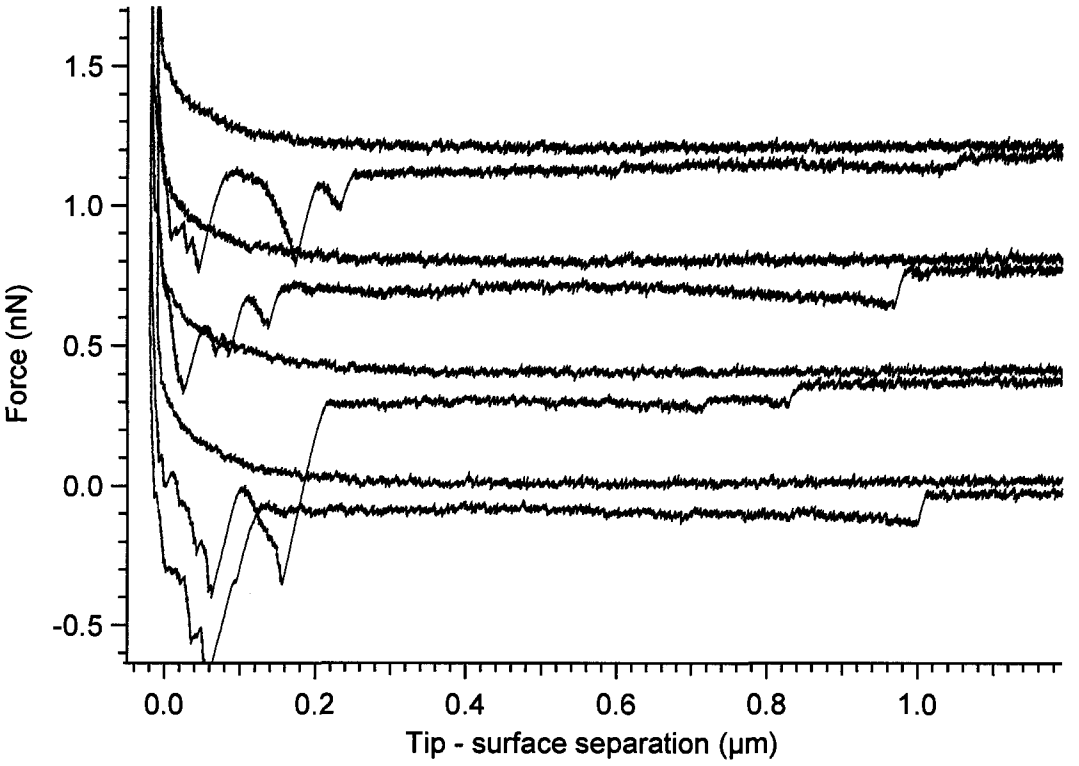

Figure 39. Typical force curves obtained with a chitosan-modified AFM tip on quartz in acetate buffer at pH 5.4

Features were observed in 35% of 184 force curves in the form of both single point desorption peaks and constant force plateaus. A schematic representation of a chitosan-modified tip interacting with a surface is shown in Figure 40.

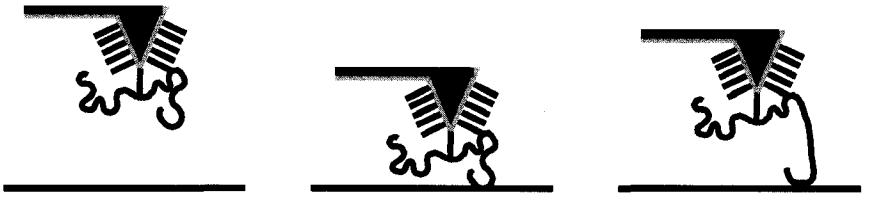

Figure 40. Schematic representation of a chitosan-modified tip interacting with a quartz surface

If the chitosan strand was only long enough to interact with the quartz surface in distinct areas, single point desorption peaks were observed. On the other hand, if the chitosan

strand was longer and able to spread on the surface, a constant force desorption plateau was recorded. It is important to note that single point desorption peaks are considered to be non-equilibrium events whereas constant force desorption plateaus are equilibrium phenomena. In the latter case, the adhesive bonds between the chitosan and the surface are being broken and formed much faster than the pulling rate. Evidence for this includes the appearance of very long constant force plateaus which suggests a flat extended conformation for these polymers adsorbed to a surface.[52] The equilibrium nature of this interaction also accounts for the absence of an expected variation in desorption force as the angle of the polymer detachment changes during the experiment. In fact, there is no change in angle during the extension since, at equilibrium, the chitosan will maximize its binding energy by sliding in the direction of the tip thus keeping the angle of the polymer relative the surface near 90°.[91]

The heights of the plateaus observed in this study were plotted in a histogram and range between 20 and 80 pN (Figure 41).

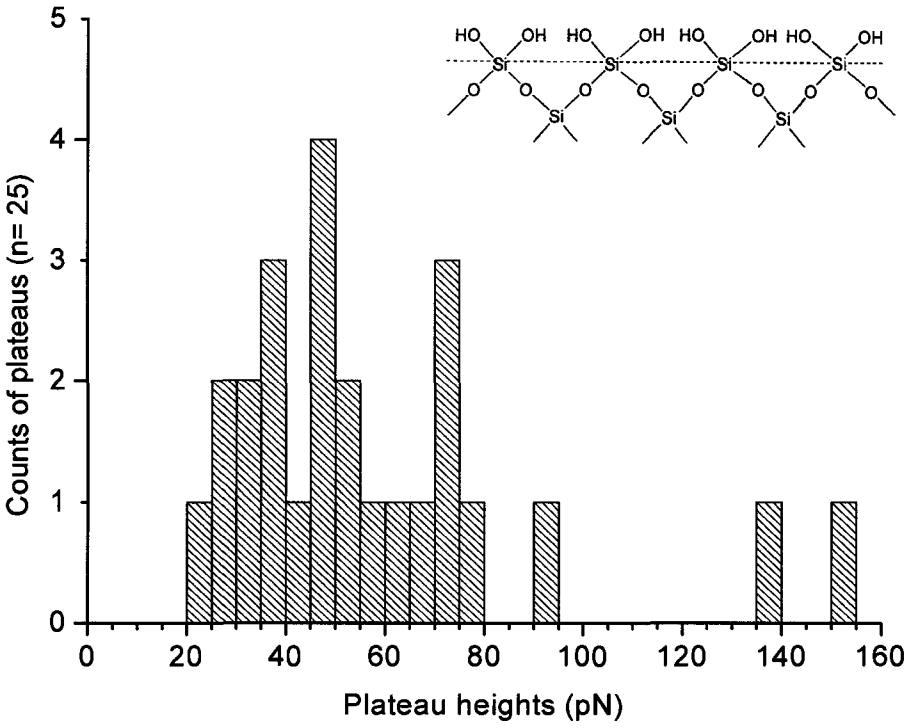

Figure 41. Plateau heights of chitosan strands desorbed from a quartz surface with a chitosan-modified AFM tip at pH 5.4

The plateau lengths of chitosan interacting with quartz were also compiled and range between 200 and 900 nm. These plateau lengths represent the chitosan strand length that is available on the modified tip to interact with the surface. The lengths of the constant force plateaus obtained are consistent with the lengths of chitosan strands observed in high resolution AFM images (Figure 25).

Quartz is a crystal composed of a lattice of silica oxide (SiO_2). Interactions at the quartz surface depend on the nature and density of surface hydroxyl groups. The ionization of these groups at the oxide-water interface follows a two step model where two consecutive protonations can take place (Figure 42).[92]

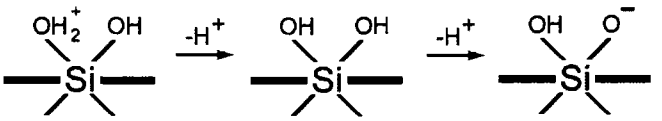

Figure 42. Two step deprotonation model at the quartz surface ($pKa_1 \sim 3$; $pKa_2 \sim 7$)

Similarly to mica and glass, the main interactions between chitosan and quartz are hydrogen bonding and electrostatic.[92] Hydrogen bonding and electrostatic interactions were also used to rationalize the adhesion of cellulose to colloidal silica particles.[93] In summary, a chitosan-modified tip was used to probe a quartz surface and interaction features similar to those on glass and mica were observed.

3.4.3. Chitosan-modified tip interactions with SAMs of dodecanethiol mixed with mercaptoundecanoic acid

A method to prove covalent attachment of molecules to surfaces is to use covalent attachment to both the tip and the surface and to look for forces representing covalent bond cleavage during SMFS experiments. This has been previously demonstrated by Grandbois *et al.* where amylose was covalently attached to a surface to which an activated AFM tip was approached. On contact, a covalent bond was formed between the activated tip and the polymer. The tip was then retracted and the covalent bond ruptured

with forces of 1.4 ± 0.3 nN for the Au-S bond and 2.0 ± 0.3 for the Si-C bond.[60] In the present study, surfaces with a SAM of DSU were prepared with the aim of testing for covalent bond cleavage. A chitosan-modified AFM tip was approached to the surface such that free chitosan strands can come into contact with the surface. The anticipated result was the covalent attachment of chitosan to the surface (*i.e.* formation of an amide bond between the amine functional groups of chitosan and the N-hydroxysuccinimidyl esters of the DSU linker molecule). If the covalent bond forms, upon tip retraction, one would expect to observe forces with magnitudes consistent with bond cleavage. The possible bonds that can be broken are: (*i*) along the chitosan molecule itself (Figure 43 d)) (*ii*) between the chitosan strand and the DSU linker at the tip or surface or (*iii*) between the gold and thiol linkage at the tip or the surface. In either of the above cases, the resulting force curve would show peak forces greater than 1 nN corresponding to covalent bond cleavage.[60]

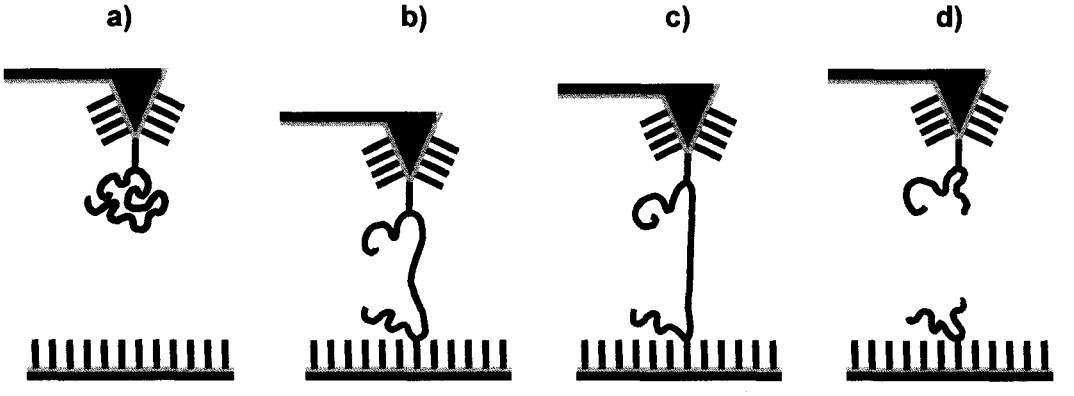

Figure 43. Covalent bond cleavage test: a) a chitosan-modified tip and a surface with a SAM of DSU, b) covalent bond formation between the amine functional group of chitosan and the DSU linker, c) retraction of the tip and d) covalent bond cleavage

When the experiment was performed, instead of observing single point high force interactions, constant force plateaus were observed (Figure 44).

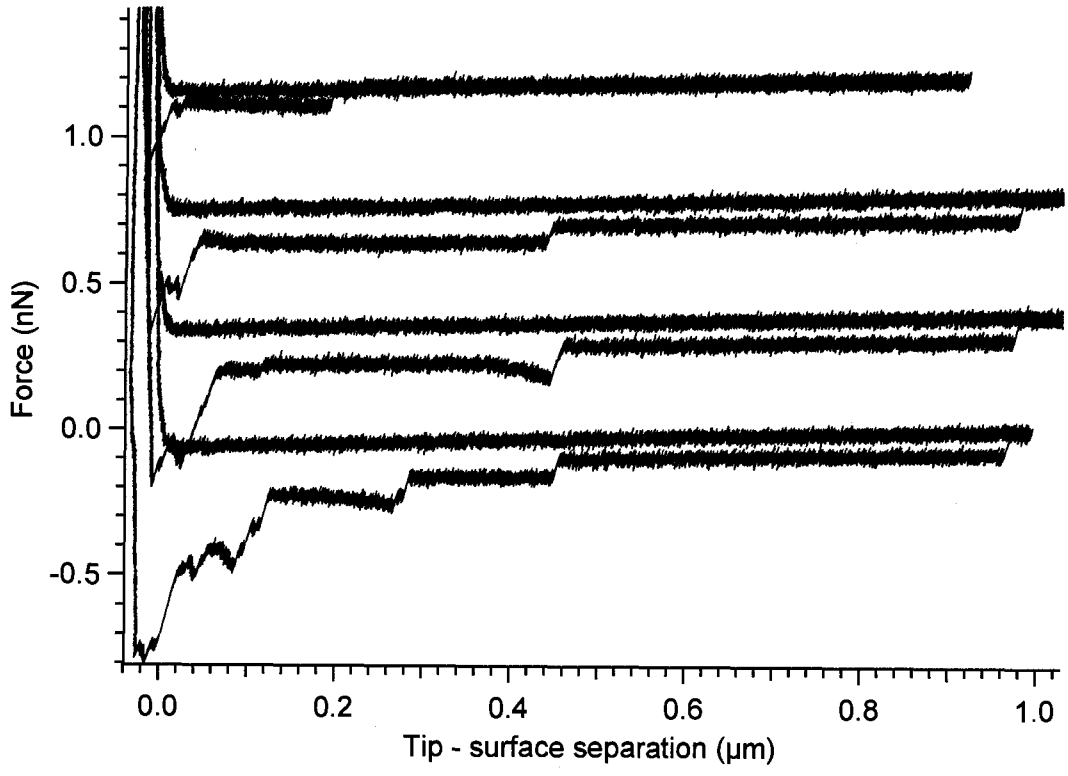

Figure 44. Typical force curves obtained with a chitosan-modified AFM tip on SAM of DSU linker in phosphate buffer at pH 7.5

The plateaus observed were of equal height suggesting constant desorption from a uniform surface. Multiple step plateaus were observed in the force curves which transpired in the histogram with force peaks ranging between 40 and 150 pN (Figure 46). These multi-step plateaus may represent consecutive chitosan desorption events from the DSU linker surface. This type of desorption is possible when several strands of chitosan interact with the surface at the same time. For example, Figure 45 shows, (*a*) three covalently bound strands of chitosan in contact with the surface, (*b*) upon retraction, all three strands desorb simultaneously from the surface resulting in a high force plateau, (*c*)

as the tip retraction continues, the shorter strands sequentially desorb resulting in step-like features in the force curve.

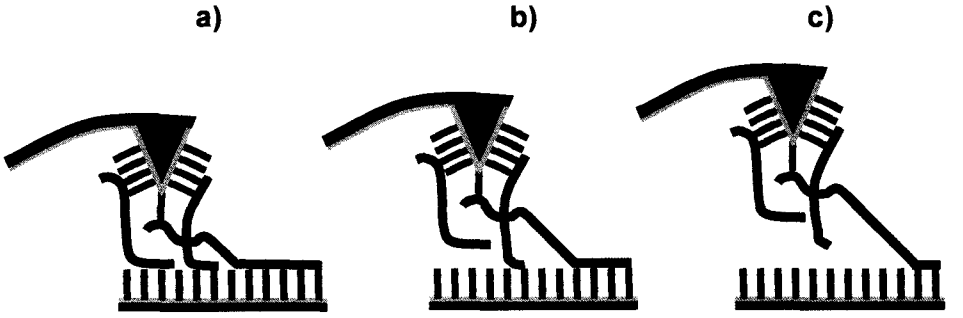

Figure 45. Schematic representation of multiple plateau desorption: a) three strands desorbing, b) shortest strand desorbed from the surface resulting in the first step in the plateau, c) second strand desorbed resulting in the second step in the plateau

Plateaus lengths are similar to those observed when a quartz surface was probed with a chitosan-modified tip (Section 3.4.2). This similarity in length suggests that in both cases, the chitosan-modified tips had similar length free dangling strands available for interaction with these surfaces.

The plateau heights neither approached nor surpassed 1 nN (Figure 46) which excludes the possibility of covalent bond cleavage expected for this experiment.

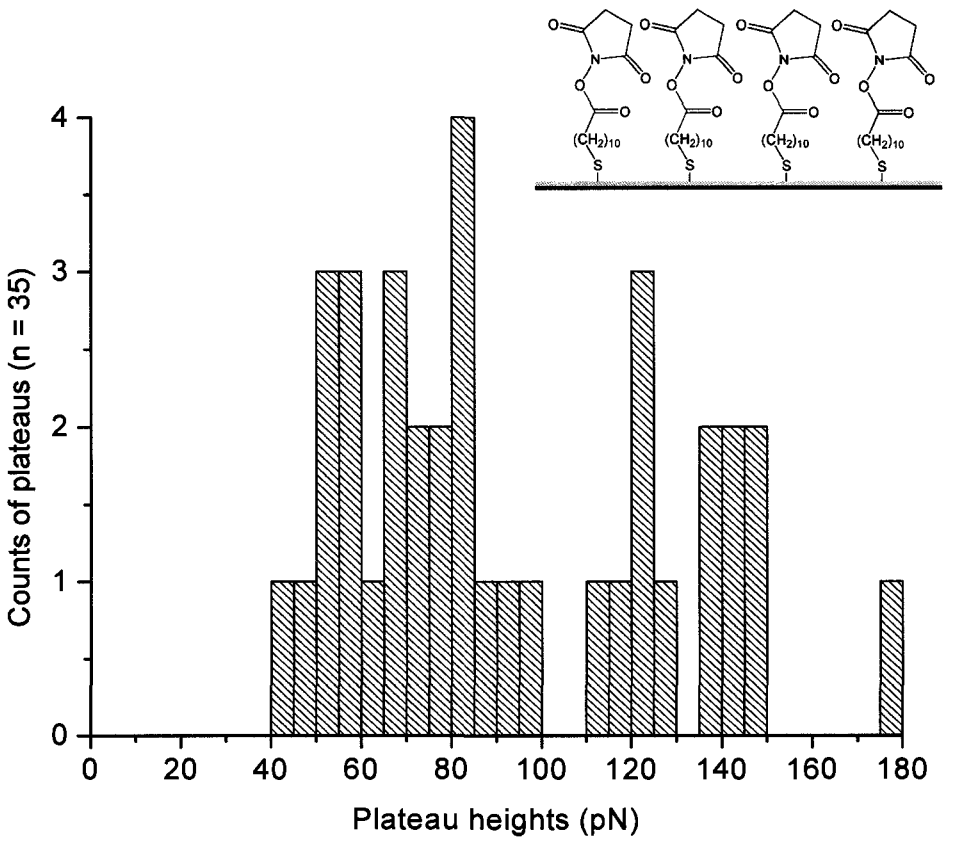

Figure 46. Plateau heights of chitosan strands desorbed from a DSU linker surface with a chitosan-modified AFM tip at pH 7.5

The lack of high force single point desorption peaks (*i.e.* bond cleavage) is due to the absence of covalent bond formation between the chitosan strand and the DSU linker. This may be due to: (*i*) the geometry of the surface (*i.e.* the decreased degrees of freedom of the reacting groups) did not allow for the reaction to take place or (*ii*) the DSU linker groups were partially hydrolyzed and were no longer reactive. The geometry of the closely packed DSU may also influence the reaction of the N-hydroxysuccinimidyl ester with the amines of chitosan. Wagner *et al.* extensively studied SAMs of DSU on gold surfaces. Their findings included poor immobilization of proteins on the monolayer (*i.e.* protein was bound to only 5% of the theoretically available binding sites on the surface)

which they attribute mostly to the limited accessibility of the succinimidyl group in the densely packed monolayer.[89,94]

The hydrolysis of some of the DSU linker molecules, which results in a terminal -COOH functional group was also suspected (Figure 47).

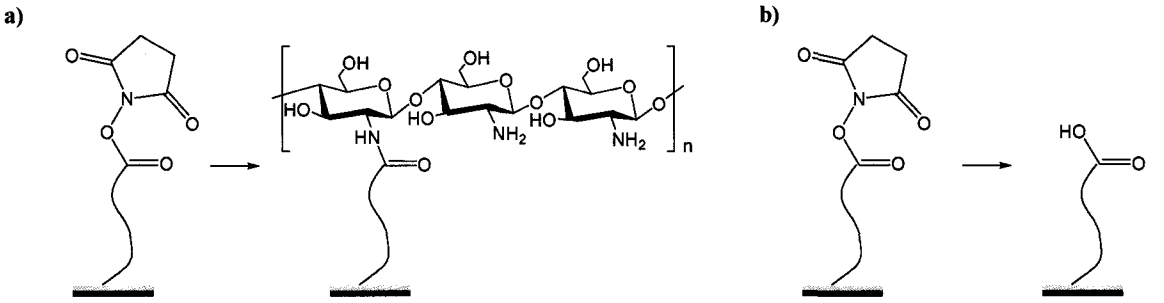

Figure 47. a) Reaction of DSU linker with chitosan, b) hydrolysis of the DSU linker

The mercaptoundecanoic acid is the end product of DSU linker hydrolysis. To test this hydrolysis hypothesis, a SAM of mercaptoundecanoic acid was prepared. The resulting force curves on this surface were lacking the expected plateaus, and instead, very high initial interaction peaks were observed. It was believed that the interaction of the numerous carboxylic acid groups on the surface with the amino groups of the chitosan-modified tip was very strong. Subsequently, it was decided to prepare diluted SAMs by mixing mercaptoundecanoic acid with dodecanethiol. When surfaces with mercaptoundecanoic acid:dodecanethiol (1:1000) were prepared and probed with a chitosan modified tip, the constant force plateau features were again prominent. Some representative force curves from the mercaptoundecanoic acid:dodecanethiol (1:1000) surface are shown in Figure 48.

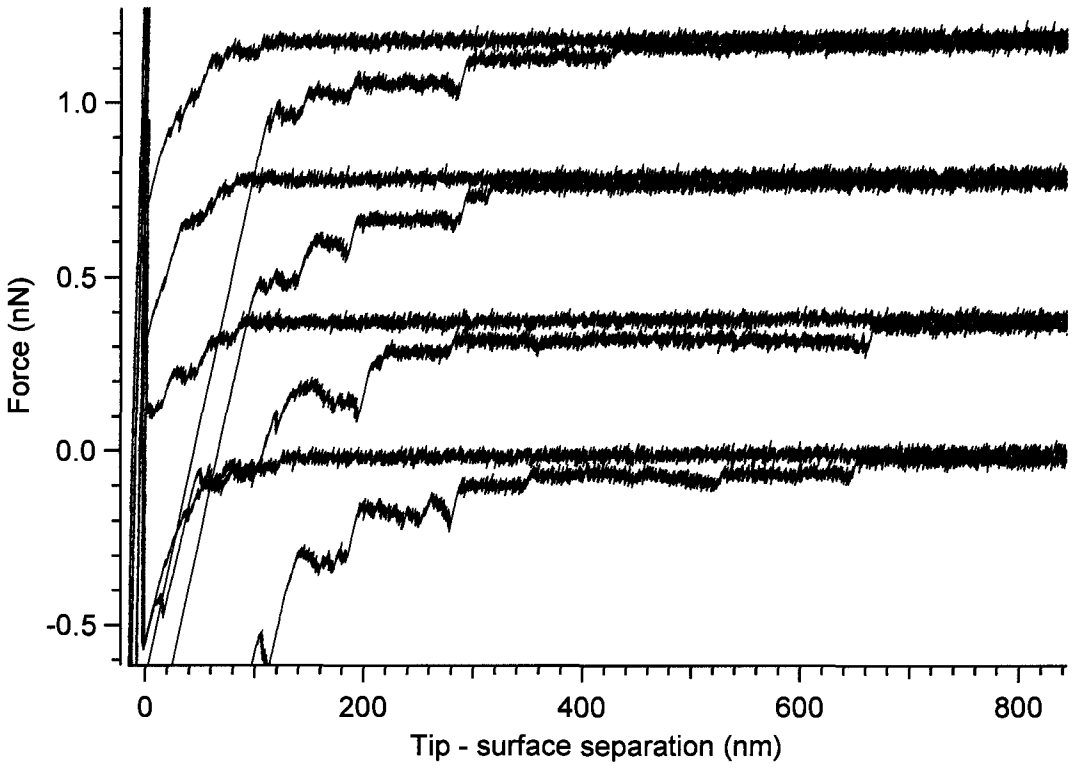

Figure 48. Typical force curves obtained with a chitosan-modified AFM tip on SAM of 1:1000 mercaptoundecanoic acid:decanethiol in acetate buffer at pH 4.5

The heights of the plateaus observed are quantized where the highest count of plateaus had an average force of 37 ± 1 pN. The second maximum occurred at approximately 71 ± 1 pN and there is evidence for a third maximum at a higher force (Figure 49).

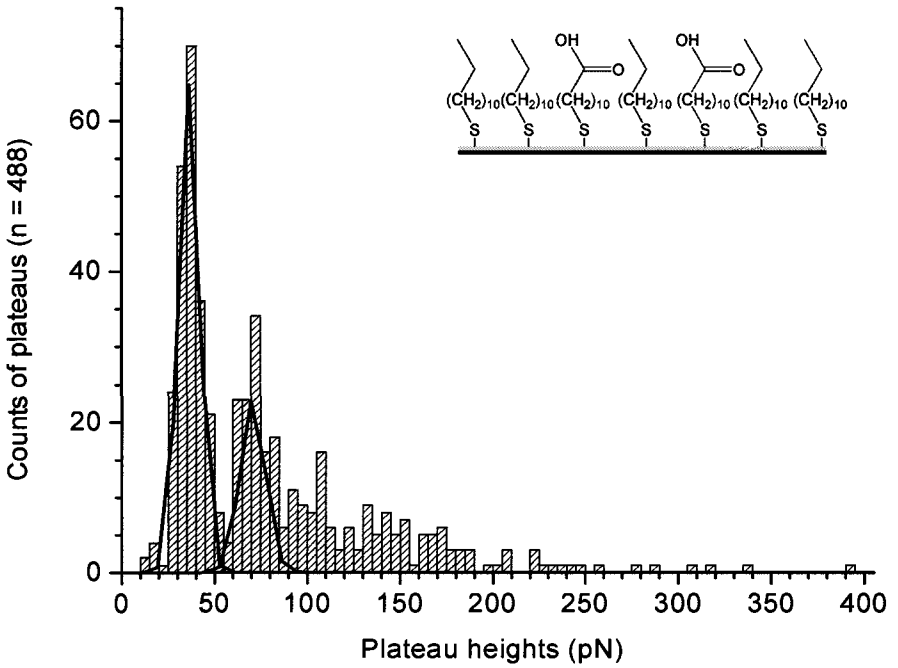

Figure 49. Plateau heights of a chitosan-modified tip on a SAM of mercaptoundecanoic acid:decanethiol (1:1000) SAM on gold. Black curve represents the best Gaussian fit of the observed forces ranging from 0 to 50 pN and 50 to 100 pN

This value corresponds to either the smallest steps observed in the force curves or the height of the last plateau which is the adhesive force of one chitosan strand to this type of surface. The constant force plateau heights are quantized and correspond to 1, 2, 3 or more chitosan strands desorbing from the surface. Desorption force curves with multiple plateaus have also been observed in the desorption experiments of hydrolyzed polyacrylamide from a silica surface[56], end-grafted poly(acrylic acid) monolayers from a silicon nitride AFM tip[95], polyacrylic acid from methyl, hydroxyl and carboxy terminated SAMs[96], cellulose from colloidal silica particles[93], carboxymethylcellulose (CMC) out of a CMC film[49] and xyloglucan molecules from a cellulose substrate.[52] The length range of the plateaus observed in this work was between 5 nm and 500 nm and again corresponds

to the length of free dangling strands on the tip available to interact with the surface. The combination of electrostatic, hydrogen bonding and van der Waals interactions between the chitosan and the SAM provides for the very uniform adhesion observed in the force curves.

3.4.4. Chitosan-modified tip interactions with PTFE

After probing surfaces where both single point desorption and constant force plateaus were observed, polytetrafluoroethylene (PTFE; Figure 50), a polymer commonly used in implants, was probed with a chitosan-modified tip.[97]

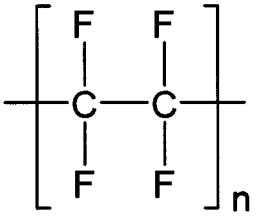

Figure 50. Chemical structure of PTFE

Desorption plateaus were observed in almost all of the force curves collected and representative examples are presented in Figure 51.

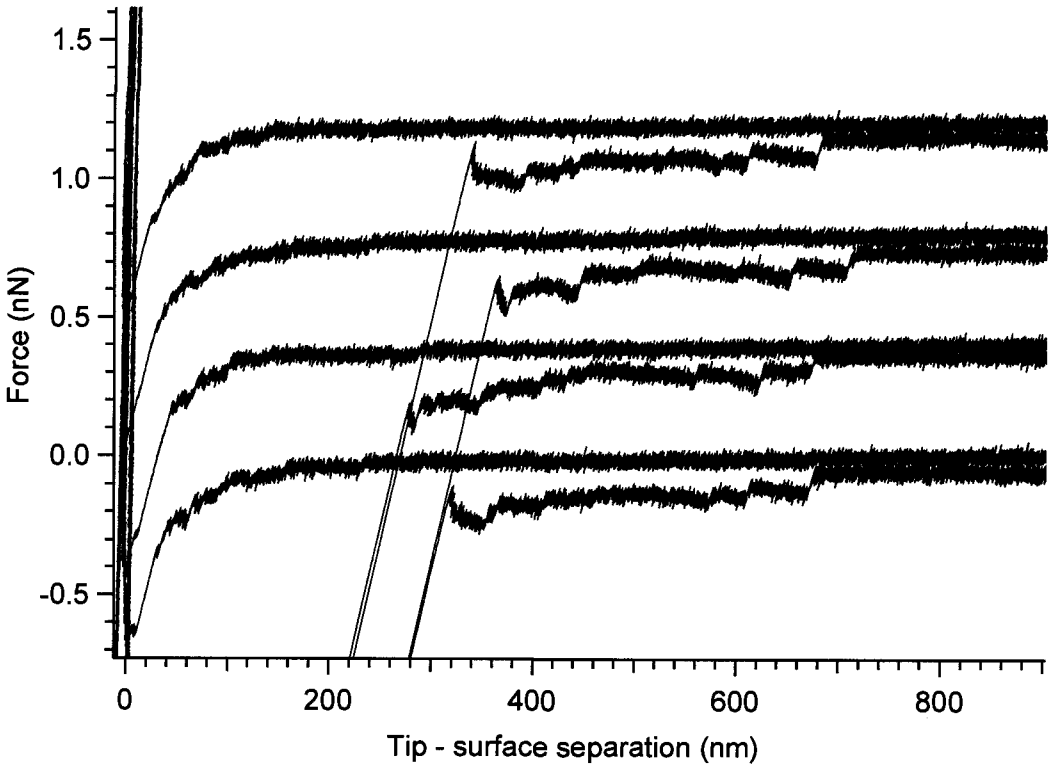

Figure 51. Typical force curves obtained with a chitosan-modified AFM tip on PTFE in acetate buffer at pH 5.4

The plateaus observed on PTFE are not as flat as those observed when chitosan interacted with mica, glass or self-assembled monolayers. This is presumably due to the roughness of PTFE which can cause inhomogeneous adhesion of the chitosan to this surface. It is well established that PTFE takes on a strong negative static charge. This strong surface charging effect plays a central role in the desorption energy of cationic chitosan from the PTFE surface.[98] Out of 142 force curves collected, almost all had multiple plateaus and a histogram of their heights in shown in (figure 62).

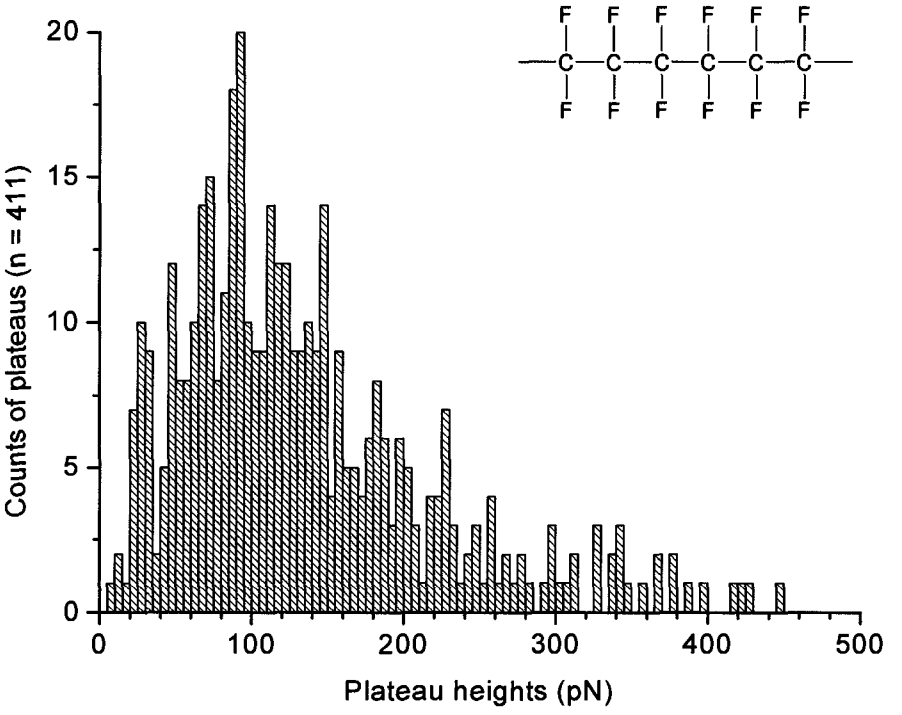

Figure 52. Plateau heights of a chitosan-modified tip on a PTFE surface

A broad range of plateau heights was observed with a maximum value at approximately 100 pN. These values are higher compared to those observed with the chitosan-modified tip interacting with the SAM of mercaptoundecanoic acid:dodecanethiol (1:1000) on gold. Because of the variability in the plateaus, further investigation of this surface is required in order to obtain more consistent values in plateau height.

3.5. Desorption energy of chitosan from different surfaces

Force curves obtained with chitosan-modified AFM tips must be used in order to determine the desorption energies of glucosamine residues with various surfaces. The

desorption energy is extracted from single molecule force spectroscopy results by calculating the area under the force extension curve and relating it to the length of the desorbed polymer (Figure 53).

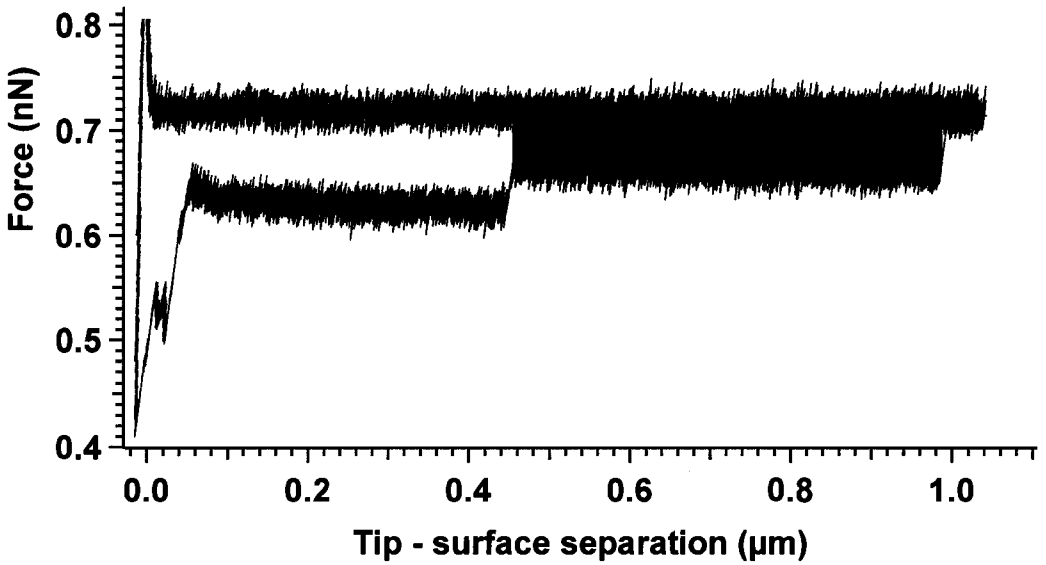

Figure 53. Calculation of desorption energy per residue is obtained by calculating the area under the last plateau (shaded region)

The total energy is divided by the number of residues present in the stretched polymer chain. Using 0.52 nm as the length of one glucosamine residue,[18,52] the magnitude of the average energies of desorption of glucosamine residues from surfaces probed in this study were calculated and are shown in Table 2.

Table 2. Average desorption energy of glucosamine residues from various surfaces (n = 5, SD = 3 x 10^{-21} J)

	Average desorption energy per glucosamine residue (J/residue)
SAM of dithiobis(succinimidylundecanoate) linker	3.9 x 10^{-20}
SAM of mercaptoundecanoic acid:dodecanethiol 1:1000	1.8 x 10^{-20}
Quartz	2.0 x 10^{-20}
Polytetrafluoroethylene (PTFE)	3.5 x 10^{-20}

The lowest chitosan desorption energy was observed on SAM of mercaptoundecanoic acid:dodecanethiol and the highest desorption energy was observed on the SAM of DSU. From a literature survey, it was found that the desorption energy of cellulosic glucose residues from hemicellulose is approximately 3.4×10^{-20} J.[52] Cellulose desorbed from silica beads with an energy of 2.1×10^{-20} J per residue whereas the energy of desorption of carboxymethylcellulose from glass was 3.9×10^{-20} J per residue.[49,93] The desorption energy values obtained in this study are comparable to those of other polysaccharides. As expected, the chemical nature of the surface being probed plays an important role in the adhesive properties of chitosan.

3.6. Mechanical properties of chitosan

Single molecule force spectroscopy was used to obtain force data and the mechanical information was extracted form individual force curves, providing values applicable to single molecules of chitosan. The mechanical constants of polymers can be determined by using mathematical models such as the Worm-Like Chain (WLC) and the Freely Jointed Chain (FJC) which are discussed in section 1.4.2. The *Contour length* (l_C) and the *Kuhn length* (l_K) are two parameters obtained from FJC fitting of force extension curves of single polymers. In the force spectroscopy experiments, l_C corresponds to the section of the molecule which is bridging between the chitosan-modified tip and the probed surface. The l_K is the parameter representing the stiffness of the polymer, in other words, l_K can be considered as the shortest inflexible segment of the polymer.

The main requirements for curve fitting are single point desorption force curves which have low noise and a baseline prior to the peak of interest. In this study, these requirements were met when probing a glass surface with a chitosan-modified AFM tip.

The peaks were detected at least 100 nm away from the surface, clearly indicating single molecule bridging between the tip and the surface. These force curves proved to be ideal candidates for curve fitting (Figure 54).

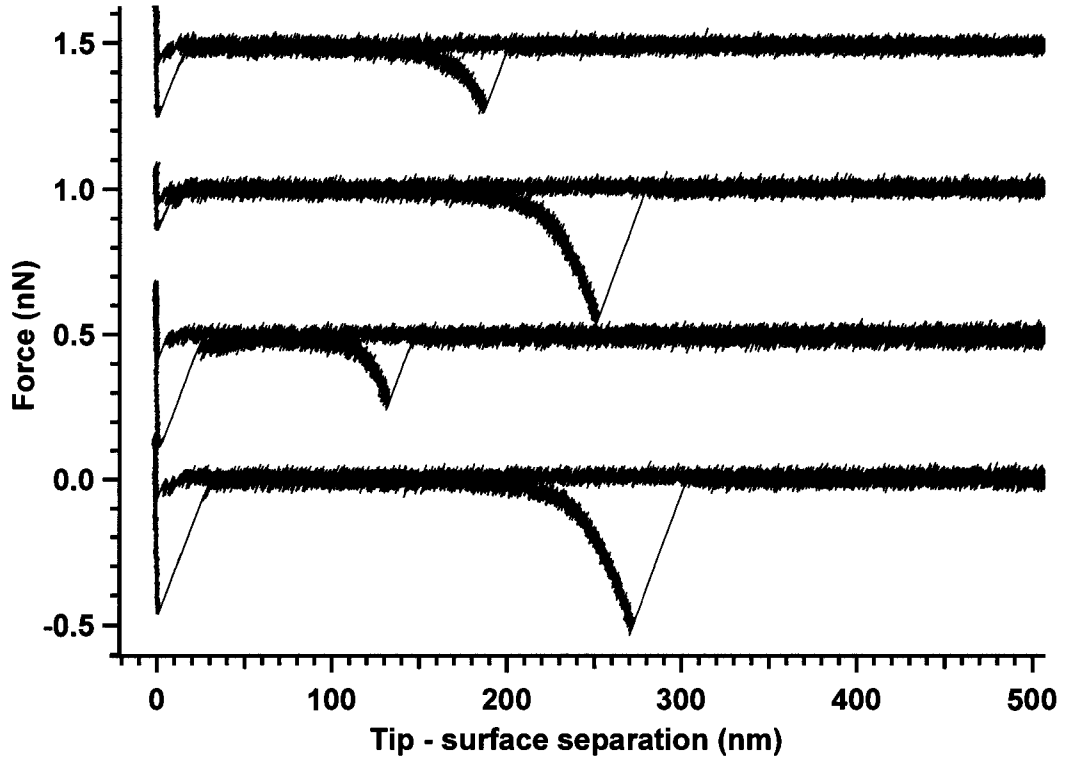

Figure 54. AFM tip with covalently attached chitosan (DDA 92%) was used to probe a glass surface in acetate buffer at pH 4.5

After smoothing the force curves, the FJC model was used to obtain the best fit of the experimental data. Increasing the l_K decreases the total number of segments of the polymer which in turn decreases the entropy. The lower entropy of the polymer results in a decreased resistance to stretching at low forces.[46] The low force regime of the force curve corresponds to the entropic component of unfolding. The FJC model is meant to fit only this region of the force curve which explains why only the initial unfolding of the chitosan strand is fit well by the FJC model (Figure 55).

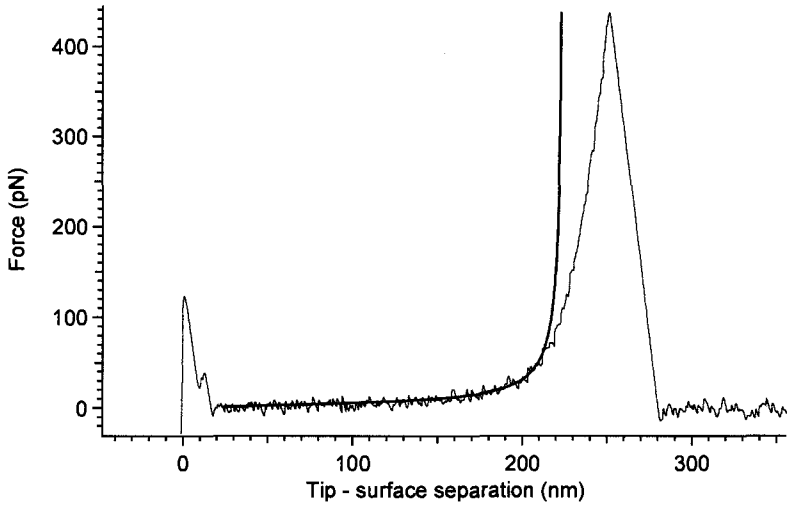

Figure 55. Example of force curve (red) fitted with a FJC model

Curve fitting using the FJC model was carried out on 14 force curves and their contour lengths ranged between 115 nm and 230 nm. The contour length corresponds to the length of the polymer strand bridging the tip to the surface. The contour length value obtained form the fitting can be validated by comparison to the location of the first increase of force in the curve. Values for l_K, the number of glucosamine units associated with l_K (i.e. one glucosamine unit = 0.52 nm)[18] and persistence length (l_P; calculated from l_K) obtained from curves fitted with the FJC are given in Table 3.

Table 3. Mechanical parameters of chitosan (DDA 92%) obtained from force curve fitting with the FJC model (n = 14)

Kuhn length (l_K) (nm)	Number of glucosamine units associated with l_K	Persistence length (l_P) (nm)
2.1 ± 0.9	4	1.1 ± 0.5

The molecular stiffness of chitosan has been extensively studied and a broad range of persistence length values were reported (4.3 to 22 nm). In 1993, Rinaudo *et al.* used intrinsic viscosity results to calculate the persistence length of chitosan and determined that it is independent of its DDA (in the range of 79% to 98%) and is 5 nm.[99] Calculations of persistence lengths based on experimental studies performed by Schatz *et al.* confirmed the non dependence of persistence length on chitosan's DDA and found values between 4.3 and 5.2 nm.[100] Berth *et al.* calculated a persistence length value of 6 nm based on average molecular masses and intrinsic viscosities determined by static light scattering, capillary viscometry and membrane osmometry.[22] Terbojevich *et al.* calculated a persistence length of 22 nm (chitosan with DDA of 58% and 85%) based on light scattering measurements[20]. Brugnerotto *et al.* used the experimental results obtained from gel permeation chromatography to determine average molecular weight distribution and to calculate a persistence length of chitosan of 9 nm[13]. In all of those studies, persistence length values are calculated based on bulk chitosan measurements. On the other hand, in the present study, chitosan stiffness values are determined for the first time from single molecule experiments. The lower values of Kuhn length obtained in this present study may be associated with the fact that in single molecule experiments, values are extracted directly from the manipulation of individual molecules whereas in bulk experiments, intramolecular interactions may affect the results obtained and influence the values of l_K observed. Kuhn lengths for chitosan (DDA 92%) were obtained from the force curves and have an average value of 2.1 ± 0.9 nm. The length of one glucosamine residue, as determined from crystallographic data, is 0.52 nm.[18] This value was used to

calculate the number of glucosamine residues corresponding to the Kuhn length *ca.* 4 (Figure 56).

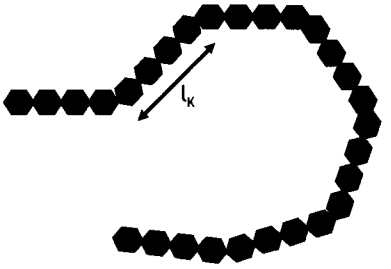

Figure 56. Schematic representation of a chitosan polymer with its calculated Kuhn length (l_K)

Compared to other polysaccharides studied by force spectroscopy techniques, chitosan's stiffness is relatively high. Amylose, has a Kuhn length of 0.45 nm[47], carboxymethyl amylose has a Kuhn length of 0.44 nm[101], dextran has a Kuhn length of 0.6 nm[102] and methylcarboxycellulose has a Kuhn length of 2.2 nm[49]. By comparing the literature values and the results of this study, chitosan is shown to be a stiffer polymer. This is likely due to the highly charged nature of chitosan (DDA 98%). The stiffness of polyelectrolytes depends on their charge density along the chain and the screening of these charges by salts in which the measurements are acquired. In chitosan, repulsive interactions arise from the charged pendant amino groups of this polymer. Furthermore, amylose and carboxymethyl amylose have much shorter Kuhn lengths than chitosan and differ from chitosan mainly in their type of monomer linkage (*i.e.* chitosan is β(1-4) linked and carboxymethyl amylose is α(1-4) linked). Methylcarboxycellulose, on the other hand, with a similar Kuhn length as chitosan, has the same β(1-4) linkage. Further investigation of α and β linked polymers at the single molecule level is needed in order to determine how the polymer stiffness is affected by the linkage between its monomers.

Chapter 4. Conclusions and future work

Chitosan adhesion on mica, glass, quartz, a variety of self-assembled monolayers and polytetrafluoroethylene were measured using AFM-based single molecules force spectroscopy. Well-defined features characteristic of single molecule adhesion and stretching were observed in the force curves:

(*i*) *Constant force desorption plateaus* provided essential information on the adhesive properties of chitosan to these surfaces. The strongest chitosan adhesion was observed on SAMs of DSU (3.94×10^{-20} J/glucosamine residue) and PTFE (3.50×10^{-20} J/glucosamine residue) whereas the weakest adhesion was observed on quartz (2.01×10^{-20} J/glucosamine residue) and on SAMs of mercaptoundecanoic acid:dodecanethiol (1:1000) (1.81×10^{-20} J/glucosamine residue).

(*ii*) *Single point desorption events* were collected and fit using the entropic FJC model. The Kuhn length for chitosan with a degree of deacetylation of 92% was 2.1 ± 0.9 nm which corresponds to a stiffness of approximately 4 glucosamine residues.

The properties of chitosan determined in this study, in the form of single molecule characteristics, provide important information regarding interactions at biointerfaces and can be applied towards the preparation of novel, chitosan-based biomaterials. For instance, characteristic plateaus observed in this work imply the strong compliance of this polymer to these surfaces. This is an important surface characteristic that could be used as a standard feature required for biomaterial testing.

SMFS allowed the determination of the adhesive behavior of chitosan to various surfaces. The trends observed upon repetitive probing of surfaces with chitosan-modified tips provide additional information about the mode of action behind these interactions.

For example, nearly identical constant force plateaus in sequential force curves (i.e. the 'peeling' and 'unpeeling' of chitosan from a glass surface (Figure 37)) show the reproducible compliance of chitosan to this surface. Ultimately this new information will contribute to the general knowledge in the field of biophysical polysaccharide research. More specifically, the single molecule mechanical markers related to polymer adhesion and stiffness are important for designing building and characterizing new chitosan-based biomaterials.

Future work will include the investigation of chitosan with varying degrees of deacetylation which is believed to be an important parameter influencing the physico-chemical properties of chitosan. Chitosan interactions with biologically relevant surfaces such as various plastics, metals and ceramics will be studied. Force curve fitting with mathematical models that include the enthalpic component of stretching will be performed to obtain additional information about the mechanical properties of this polymer. Finally, AFM probes modified with microscopic beads will be used to perform SMFS experiments. The geometry obtained from such probes mimics that of two flat surfaces and might provide useful information about chitosan desorption.

References

(1) Robyt, J. F. *Essentials of Carbohydrate Chemistry*; Sprigner-Verlag: New York, 1998.

(2) Lindhorst, T. K.; Albertina, C. *Essentials of Carbohydrate Chemistry and Biochemistry*; Wiley-VCH: Weinheim, 2003.

(3) Marszalek, P.; Li, H.; Fernandez, J. M. *Nat. Biotechnol.* **2001**, *19*, 258-262.

(4) Davis, B. G.; Fairbanks, A. J. *Carbohydrate Chemistry*; Oxford: New York, 2002.

(5) Muzzarelli, R. A. A. *Chitin*; Pergamon Press, 1977.

(6) Suh, J. K.; Matthew, H. W. *Biomaterials* **2000**, *21*, 2589-2598.

(7) Bumgardner, J. D.; Wiser, R.; Elder, S. H.; Jouett, R.; Yang, Y.; Ong, J. L. *J. Biomater. Sci., Polym. Ed.* **2003**, *14*, 1401-1409.

(8) Bumgardner, J. D.; Wiser, R.; Gerard, P. D.; Bergin, P.; Chestnutt, B.; Marini, M.; Ramsey, V.; Elder, S. H.; Gilbert, J. A. *J. Biomater. Sci., Polym. Ed.* **2003**, *14*, 423-438.

(9) Lavertu, M.; Methot, S.; Tran-Khanh, N.; Buschmann, M. D. *Biomaterials* **2006**, *27*, 4815-4824.

(10) Ruel-Gariepy, E.; Chenite, A.; Chaput, C.; Guirguis, S.; Leroux, J. C. *Int. J. Pharm.* **2000**, *203*, 89-98.

(11) Kujawa, P.; Schmauch, G.; Viitala, T.; Badia, A.; Winnik, F. M. *Biomacromolecules* **2007**, *8*, 3169-3176.

(12) Lavertu, M.; Xia, Z.; Serreqi, A. N.; Berrada, M.; Rodrigues, A.; Wang, D.; Buschmann, M. D.; Gupta, A. *J. Pharm. Biomed. Anal.* **2003**, *32*, 1149-1158.

(13) Brugnerotto, J.; Desbrieres, J.; Heux, L.; Mazeau, K.; Rinaudo, M. *Macromol. Symp.* **2001**, *168*, 1-20.

(14) Brugnerotto, J.; Desbrieres, J.; Roberts, G.; Rinaudo, M. *Polymer* **2001**, *42*, 9921-9927.

(15) Sorlier, P.; Denuziere, A.; Viton, C.; Domard, A. *Biomacromolecules* **2001**, *2*, 765-772.

(16) Yi, H.; Wu, L.-Q.; Bentley, W. E.; Ghodssi, R.; Rubloff, G. W.; Culver, J. N.; Payne, G. F. *Biomacromolecules* **2005**, *6*, 2881-2894.

(17) Hoemann, C. D.; Hurtig, M.; Rossomacha, E.; Sun, J.; Chevrier, A.; Shive, M. S.; Buschmann, M. D. *J Bone Joint Surg* **2005**, *87*, 2671-2686.

(18) Filion, D.; Lavertu, M.; Buschmann, M. D. *Biomacromolecules* **2007**, *8*, 3224-3234.

(19) No, H. K.; Lee, K. S.; Meyers, S. P. *J. Food Sci.* **2000**, *65*, 1134-1137.

(20) Terbojevich, M.; Cosani, A.; Conio, G.; Marsano, E.; Bianchi, E. *Carbohydr. Res.* **1991**, *209*, 251-260.

(21) Lazaridis, N. K.; Kyzas, G. Z.; Vassiliou, A. A.; Bikiaris, D. N. *Langmuir* **2007**, *23*, 7634-7643.

(22) Berth, G.; Dautzenberg, H.; Peter, M., G. *Carbohydr. Polym.* **1998**, *36*, 205-216.

(23) Bustamante, C.; Macosko, J. C.; Wuite, G. J. L. *Nat. Rev. Mol. Cell Biol.* **2000**, *1*, 130-136.

(24) Clausen-Schaumann, H.; Seitz, M.; Krautbauer, R.; Gaub, H. E. *Curr. Opin. Chem. Biol.* **2000**, *4*, 524-530.
(25) Ashkin, A.; Dziedzic, J. M.; Bjorkholm, J. E.; Chu, S. *Opt. Lett.* **1986**, *11*, 288-290.
(26) Wiliams, C. M. In *Biophysics Textbook Online*; DeFelice, L., Ed.; Biophysical Society: Bethesda, 2002; Vol. Single Molecule Techniques, pp 1-14.
(27) Kellermayer, M. S. Z.; Smith, S. B.; Granzier, H. L.; Bustamante, C. *Science* **1997**, *276*, 1112-1116.
(28) Onoa, B.; Dumont, S.; Liphardt, J.; Smith, S. B.; Tinoco, I., Jr.; Bustamante, C. *Science* **2003**, *299*, 1892-1896.
(29) Smith, S. B.; Finzi, L.; Bustamante, C. *Science* **1992**, *258*, 1122-1126.
(30) Tabor, D.; Winterton, R. H. S. *Nature (London, U. K.)* **1968**, *219*, 1120-1121.
(31) Israelachvili, J. N.; Adams, G. E. *Journal of the Chemical Society, Faraday Transactions 1: Physical Chemistry in Condensed Phases* **1978**, *74*, 975-1001.
(32) Israelachvili, J. N.; Tabor, D. *Proceedings of the Royal Society of London, Series A: Mathematical, Physical and Engineering Sciences* **1972**, *331*, 19-38.
(33) Schob, A.; Cichos, F. *J. Phys. Chem. B* **2006**, *110*, 4354-4358.
(34) Kamimura, S.; Takahashi, K. *Nature (London, U. K.)* **1981**, *293*, 566-568.
(35) Kishino, A.; Yanagida, T. *Nature (London, U. K.)* **1988**, *334*, 74-76.
(36) Binnig, G.; Rohrer, H. *Helvetica Physica Acta* **1982**, *55*, 726-735.
(37) Binnig, G.; Rohrer, H.; Gerber, C.; Weibel, E. *Appl. Phys. Lett.* **1982**, *40*, 178-180.
(38) Binnig, G.; Quate, C. F.; Gerber, C. *Phys. Rev. Lett.* **1986**, *56*, 930.
(39) Sader, J. E.; Chon, J. W. M.; Mulvaney, P. *Rev. Sci. Instrum.* **1999**, *70*, 3967-3969.
(40) Sader, J. E.; Larson, I.; Mulvaney, P.; White, L. R. *Rev. Sci. Instrum.* **1995**, *66*, 3789-3798.
(41) Sader, J. E. In *Encyclopedia of Surface and Colloid Science*; Dekker, M., Ed., 2002; Vol. x, pp 846-856.
(42) Takano, H.; Kenseth, J. R.; Wong, S.-S.; O'Brien, J. C.; Porter, M. D. *Chem. Rev.* **1999**, *99*, 2845-2890.
(43) Steed, J. W.; Atwood, J. L. *Supramolecular Chemistry: A Concise Introduction*; Wiley-VCH, 2000.
(44) Price, N. C.; Dwek, R. A. *Principles and Problems of Physical Chemistry for Biochemists*, 1982.
(45) Lee, G.; Nowak, W.; Jaroniec, J.; Zhang, Q.; Marszalek Piotr, E. *Biophys. J.* **2004**, *87*, 1456-1465.
(46) Fisher, T. E.; Marszalek, P. E.; Oberhauser, A. F.; Carrion-Vazquez, M.; Fernandez, J. M. *Journal of Physiology (Cambridge, United Kingdom)* **1999**, *520*, 5-14.
(47) Marszalek, P. E.; Oberhauser, A. F.; Pang, Y.-P.; Fernandez, J. M. *Nature (London, U. K.)* **1998**, *396*, 661-664.
(48) Marszalek, P. E.; Pang, Y.-P.; Li, H.; El Yazal, J.; Oberhauser, A. F.; Fernandez, J. M. *Proc. Natl. Acad. Sci. U. S. A.* **1999**, *96*, 7894-7898.
(49) Scherer, A.; Zhou, C.; Michaelis, J.; Brauchle, C.; Zumbusch, A. *Macromolecules* **2005**, *38*, 9821-9825.

(50) Seitz, M.; Friedsam, C.; Jostl, W.; Hugel, T.; Gaub Hermann, E. *ChemPhysChem* **2003**, *4*, 986-990.
(51) Conti, M.; Bustanji, Y.; Falini, G.; Ferruti, P.; Stefoni, S.; Samori, B. *ChemPhysChem* **2001**, *2*, 610-613.
(52) Morris, S.; Hanna, S.; Miles, M. J. *Nanotechnology* **2004**, *15*, 1296-1301.
(53) Sonnenberg, L.; Parvole, J.; Kuehner, F.; Billon, L.; Gaub, H. E. *Langmuir* **2007**, *23*, 6660-6666.
(54) Friedsam, C.; Del Campo Becares, A.; Jonas, U.; Seitz, M.; Gaub, H. E. *New Journal of Physics* **2004**, *6*, 1-16.
(55) Balasundaram, G.; Webster, T. J. *J. Mater. Chem.* **2006**, *16*, 3737-3745.
(56) Long, J.; Xu, Z.; Masliyah, J. H. *Langmuir* **2006**, *22*, 1652-1659.
(57) Graham, J. S.; Phillips, C. L.; Grandbois, M. *Physics in Canada* **2004**, *60*, 157-164.
(58) Janshoff, A.; Neitzert, M.; Oberdorfer, Y.; Fuchs, H. *Angew. Chem., Int. Ed.* **2000**, *39*, 3212-3237.
(59) Lee, G. U.; Chrisey, L. A.; Colton, R. J. *Science* **1994**, *266*, 771-773.
(60) Grandbois, M.; Beyer, M.; Rief, M.; Clausen-Schaumann, H.; Gaub, H. E. *Science* **1999**, *283*, 1727-1730.
(61) Li, H.; Rief, M.; Oesterhelt, F.; Gaub, H. E. *Appl. Phys. A: Mater. Sci. Process.* **1999**, *68*, 407-410.
(62) Rief, M.; Clausen-Schaumann, H.; Gaub, H. E. *Nat. Struct. Biol.* **1999**, *6*, 346-349.
(63) Vander Wal, M.; Kamper, S.; Headley, J.; Sinniah, K. *Langmuir* **2006**, *22*, 882-886.
(64) Rief, M.; Gautel, M.; Oesterhelt, F.; Fernandez, J. M.; Gaub, H. E. *Science* **1997**, *276*, 1109-1112.
(65) Muller, D. J.; Baumeister, W.; Engel, A. *Proc. Natl. Acad. Sci. U. S. A.* **1999**, *96*, 13170-13174.
(66) Oesterhelt, F.; Oesterhelt, D.; Pfeiffer, M.; Engel, A.; Gaub, H. E.; Muller, D. J. *Science* **2000**, *288*, 143-146.
(67) Zhang, Q.; Marszalek, P. E. *J. Am. Chem. Soc.* **2006**, *128*, 5596-5597.
(68) Li, H. B.; Rief, M.; Oesterhelt, F.; Gaub, H. E. *Adv. Mater.* **1998**, *10*, 316-319.
(69) Cai, K.; Bossert, J.; Jandt, K. D. *Colloids Surf., B* **2006**, *49*, 136-144.
(70) Agheli, H.; Malmstroem, J.; Hanarp, P.; Sutherland, D. S. *Mater. Sci. Eng., C* **2006**, *26*, 911-917.
(71) Kennedy, S. B.; Washburn, N. R.; Simon, C. G.; Amis, E. J. *Biomaterials* **2006**, *27*, 3817-3824.
(72) Katti, K. S. *Colloids Surf., B* **2004**, *39*, 133-142.
(73) Noy, A. *Surf. Interface Anal.* **2006**, *38*, 1429-1441.
(74) Jagur-Grodzinski, J. *Polym. Adv. Technol.* **2006**, *17*, 395-418.
(75) Puleo, D. A.; Nanci, A. *Biomaterials* **1999**, *20*, 2311-2321.
(76) Stevens, M. M.; George, J. H. *Science* **2005**, *310*, 1135-1138.
(77) Hermanson, G. T.; Editor. *Bioconjugate Techniques*, 1995.
(78) Cevc, G., Ed. *Phospholipids Handbook*; Marcel Dekker, Inc.: New York, 1993.
(79) Hoerber, J. K. H.; Miles, M. J. *Science* **2003**, *302*, 1002-1005.

(80) Lo, Y.-S.; Huefner, N. D.; Chan, W. S.; Dryden, P.; Hagenhoff, B.; Beebe, T. P., Jr. *Langmuir* **1999**, *15*, 6522-6526.
(81) Weeks, B. L.; Vaughn, M. W.; DeYoreo, J. J. *Langmuir* **2005**, *21*, 8096-8098.
(82) Scoog, D. A.; Holler, J. F.; Nieman, T. A. *Principles of Instrumental Analysis*, Fifth ed.; Thomson Learning Inc.: Toronto, 1998.
(83) Chupa, J. M.; Foster, A. M.; Sumner, S. R.; Madihally, S. V.; Matthew, H. W. T. *Biomaterials* **2000**, *21*, 2315-2322.
(84) Kuttel, M.; Naidoo, K. J. *J. Am. Chem. Soc.* **2005**, *127*, 12-13.
(85) Roiter, Y.; Minko, S. *J. Phys. Chem. B* **2007**, *111*, 8597-8604.
(86) Abu-Lail, N. I.; Camesano, T. A. *Journal of Microscopy (Oxford, United Kingdom)* **2003**, *212*, 217-238.
(87) Kacher, C. M.; Weiss, I. M.; Stewart, R. J.; Schmidt, C. F.; Hansma, P. K.; Radmacher, M.; Fritz, M. *Eur. Biophys. J.* **2000**, *28*, 611-620.
(88) Butt, H.-J.; Cappella, B.; Kappl, M. *Surf. Sci. Rep.* **2005**, *59*, 1-152.
(89) Wagner, P.; Zaugg, F.; Kernen, P.; Hegner, M.; Semenza, G. *J. Vac. Sci. Technol., B* **1996**, *14*, 1466-1471.
(90) Corning Inc. (Lowell, M.
(91) Kuehner, F.; Erdmann, M.; Sonnenberg, L.; Serr, A.; Morfill, J.; Gaub, H. E. *Langmuir* **2006**, *22*, 11180-11186.
(92) Duval, Y.; Mielczarski, J. A.; Pokrovsky, O. S.; Mielczarski, E.; Ehrhardt, J. J. *J. Phys. Chem. B* **2002**, *106*, 2937-2945.
(93) Radtchenko, I. L.; Papastavrou, G.; Borkovec, M. *Biomacromolecules* **2005**, *6*, 3057-3066.
(94) Wagner, P.; Hegner, M.; Kernen, P.; Zaugg, F.; Semenza, G. *Biophys. J.* **1996**, *70*, 2052-2066.
(95) Sonnenberg, L.; Parvole, J.; Borisov, O.; Billon, L.; Gaub, H. E.; Seitz, M. *Macromolecules* **2006**, *39*, 281-288.
(96) Friedsam, C.; Gaub, H. E.; Netz, R. R. *Biointerphases* **2006**, *1*, MR1-MR21.
(97) Werner, C.; Maitz, M. F.; Sperling, C. *J. Mater. Chem.* **2007**, *17*, 3376-3384.
(98) Rijnaarts, H. H. M.; Norde, W.; Bouwer, E. J.; Lyklema, J.; Zehnder, A. J. B. *Appl. Environ. Microbiol.* **1993**, *59*, 3255-3265.
(99) Rinaudo, M.; Milas, M.; Le Dung, P. *Int. J. Biol. Macromol.* **1993**, *15*, 281-285.
(100) Schatz, C.; Viton, C.; Delair, T.; Pichot, C.; Domard, A. *Biomacromolecules* **2003**, *4*, 641-648.
(101) Kuhner, F.; Erdmann, M.; Gaub, H. E. *Phys. Rev. Lett.* **2006**, *97*, 1-4.
(102) Rief, M.; Oesterhelt, F.; Heymann, B.; Gaub, H. E. *Science* **1997**, *275*, 1295-1297.